J Mater Sci (2019) 54:7131–7155

Energy materials

Dielectric relaxations and transport properties parameter analysis of novel blended solid polymer electrolyte for sodium-ion rechargeable batteries

Pritam[1], Anil Arya[1], and A. L. Sharma[1,*]

[1] *Department of Physical Sciences, Central University of Punjab, Bathinda, Punjab 151001, India*

Received: 29 November 2018
Accepted: 18 January 2019
Published online: 29 January 2019

ABSTRACT

A novel blended solid polymer electrolyte comprising polyethylene oxide and polyvinylpyrrolidone polymers for blending and sodium nitrate ($NaNO_3$) as ion conducting species has been optimized via standard solution-cast technique. XRD, FESEM, and FTIR were performed to obtain the information about the structural changes, morphology, and microstructural changes (polymer–ion and ion–ion interactions) of the solid polymer electrolyte films. The electrochemical impedance spectroscopy, linear sweep voltammetry, and *i*–*t* characteristics were performed to evaluate the ionic conductivity, voltage stability window, and ion transference number. The impedance study was done in a broad temperature range (40–100 °C). The DSC and TGA were used to obtain information about the thermal transitions and thermal stability of prepared films. The ion dynamics is further investigated by analyzing the complex permittivity, loss tangent, and complex conductivity. All the plots were fitted through established theoretical model/expressions in whole frequency window to obtain dielectric strength, ion conduction path behavior, and relaxation time. Transport parameters such as number density (n), mobility (μ), and diffusion coefficient (D) of mobile ions were obtained by three methods and compared satisfactorily. Lastly, a coherent mechanism for the migration of charge transport carriers within the solid polymer composites has been proposed based on the performed experimental outcome.

Introduction

In view of collective demand of energy worldwide and exhaustion of the traditional energy resources (fossil fuels, coal, etc.), it becomes mandatory to develop the clean and renewable (C&R) resources for application in the transport and portable electronic sectors. The most appropriate energy source is the Li-ion battery (LIB) technology, which is chosen due to its high specific energy density, broad electrochemical potential window, a prolonged service life, and no memory loss. However, the limited availability of the

Address correspondence to E-mail: alsharma@cup.edu.in

https://doi.org/10.1007/s10853-019-03381-3

lithium metal and high price force the researchers to develop its alternative. Therefore, research in the field keeps trying parallel development of secondary batteries which could be able to fulfill the desire of Li-associated energy storage device and could be able to eliminate the hurdle associated with it. In this line, the most feasible and competitive element that has the potential to replace lithium (Li) is sodium (Na). It could be possible due to its high abundance (1000 times more than Li), low toxicity, lower price, voltage versus SHE (2.7 V), and no geographical boundaries. Recently, again there is huge work carrying on all over the world to develop sodium-ion batteries (SIB) [1–4].

As any rechargeable battery consists of four components as (1) cathode, (2) anode, (3) electrolyte, and (4) separator, during the transportation of charge carrier, ions are shuttled between the two electrodes via the electrolyte and separator prevents the physical contact of electrodes to avoid from short-circuiting. Electrolyte provides the path for conduction and plays a tremendous role during charging/discharging operation. It seems that electrolyte is a crucial component of any rechargeable battery system. The existing battery technology is based on the electrolyte consisting of organic/inorganic separator pored with ionic liquids (like $LiPF_6$) that challenges the safety issues on every step in terms of volatility, leakage, reaction with electrodes, and flammability. In this way, it becomes mandatory to eliminate the above-said issues to fulfill the dream of a safe/stable secondary battery system [5].

Research and development of polymer electrolytes (PEs) have gained the interest of the scientific community as an alternative of the traditional liquid-based electrolytes due to advantages such as light-weight, flexibility, geometric stability, improved safety, and no leakage [6, 7]. Firstly, the gel polymer electrolyte (GPE) was developed by the addition of organic solvent as a plasticizer (such as EC, PC, DEC) in polymer salt matrix and displayed improved properties as compared to the liquid electrolyte. But, poor mechanical property and interfacial issues prevented their use for the safe battery system. Solid polymer electrolyte (SPE) films seem to be the best alternative and have the potential to eliminate all the above-said issues of the traditional and gel polymer electrolyte system. The major advantage with the SPE is simple and low-cost design strategy, flexibility, and miniaturization of devices that automatically lowers both cost and weight. As no liquid part is used, so all solid-state battery guarantees great safety with respect to existing one. The desirable properties for SPE are high ionic conductivity, broad operating voltage, and desirable mechanical, thermal and interfacial properties. One more important advantage of SPE become essential to mention here that it could be able to serve the dual purpose of electrolyte and separator in any such energy storage/conversion devices [7–12].

Some recently published works reported the exploration of SPEs for the application in battery to employ various compositions, i.e., poly (vinylidene fluoride-hexafluoropropylene) [P(VdF-co-HFP)] [13], polyethylene oxide (PEO) [14], polyvinylpyrrolidone (PVP) [15], PAN [16, 17], poly (vinyl alcohol)/poly (vinylpyrrolidone) (PVA/PVP) [18], PVA–PMMA [19], and PEO–PAN [20–22]. In aforementioned system combination, polyethylene oxide (PEO) gains more attention as a host polymer due to its wide range of properties like the good capability of complex formation with many salts, high ionic conductivity, and the presence of electron-rich ether group in polymer backbone (CH_2–O–CH_2). However, its semicrystalline nature results in low ionic conductivity and prevents its use in such application. In order to remove this drawback of PEO, there are various approaches (like polymer blending, cross-linking, etc.) have been adopted to suppress its crystallinity. In adopted approaches, polymer blending seems more convincing and effective, as polymer blending combined and improved the properties as compared with individual host polymer. The most common interaction existing in polymer blends is (1) hydrogen bonding, (2) dipole–dipole interactions, and (3) ionic interactions [23]. The best polymer for blending is the poly (vinylpyrrolidone) (PVP) due to high amorphous content and presence of rigid pyrrolidone group and carbonyl group (C=O). The former one promotes faster ion dynamics, while latter one promotes the possibility of complex formation with various inorganic salts [24–27].

Recently, a few investigations have been carried out to prepare solid polymer electrolyte using different sodium salts [26, 28–33]. Our group also investigated the blend of solid polymer electrolyte based on PEO–PVP + $NaPF_6$. It demonstrated the improved electrochemical properties as compared to the other sodium salts [27]. To the best of our

knowledge, there is no report on the preparation and characterization of blend solid polymer electrolyte with sodium nitrate salt in a wide range of composition. Hence, the present investigation is the extension of the investigation of different sodium salts in view of the exploration of appropriate and compatible solid polymeric separator required for such devices. Herein, we report the simple preparation of blend solid polymer electrolyte (BSPE) based on polyethylene oxide (PEO), polyvinylpyrrolidone (PVP)-blended matrix complexes with sodium nitrate ($NaNO_3$) as aprotic salt. The structural, microstructural, morphological, electrochemical, transport and dielectric properties are investigated in detail followed by the correlation between the above results. On the basis of the experimental results, an ion-transport mechanism has been proposed to visualize the obtained results in a simple and logical manner.

Preparation of BSPE films

Blended solid polymer electrolyte has been prepared by the solution-cast technique. First of all, the polyethylene oxide (PEO; 0.4 g) and polyvinylpyrrolidone (PVP; 0.1 g) (Aldrich) are added with methanol (Aldrich) in the required wt%, and the solution is stirred till a homogenous solution is obtained. Figure 1a shows the interaction between the two polymers. Then, the salt is added in the stoichiometric ratio (O/Na = 2, 4, 6, 8, 10, 12, 14, 16, 20) to the blend polymer solution, and solution is stirred again till a transparent solution is obtained. Then the solution is cast in the Teflon Petri dishes and allowed to evaporate slowly followed by vacuum drying. Finally, a freestanding polymer film is obtained and kept is vacuum desiccator (with silica gel) for further characterization. The average thickness of the films was ~ 100 to 120 μm measured using micrometer (Digimatic Micrometer, Mitutoyo). Figure 1b shows the interactions between the blend polymer and salt.

Characterization techniques

The structural investigations were obtained by X-ray diffraction (XRD) (Malvern Panalytical) with CuK_α radiation (λ = 1.54 Å) in the Braggs angle range (2θ) from 10° to 60°. The morphological properties are obtained using the field emission scanning electron microscopy (FESEM) (Carl Zeiss product). The microstructural and presence of interaction among the different component of the PNC are obtained through Fourier transform infrared (FTIR) spectroscopy (Model: Bruker Tensor 27, Model: NEXUS–870) recorded in absorbance mode in the wavenumber region 600–3000 cm^{-1} with a resolution of 4 cm^{-1}.

The impedance spectroscopy has been performed using the electrochemical analyzer (CHI760, USA) in the frequency range of 1 Hz–1 MHz and temperature range of 40–100 °C (Temperature Controller; Marine

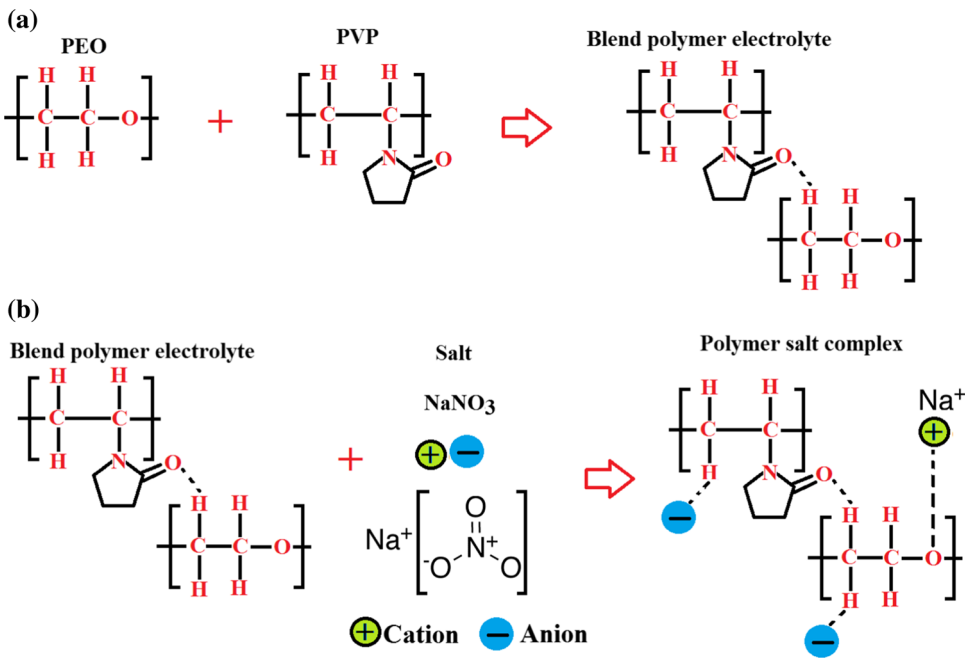

Figure 1 **a** Blend polymer electrolyte formation and **b** polymer salt complex formation.

India). An AC signal of 20 mV is applied across the cell configuration SS|BSPE|SS. Here, SS refers to stainless-steel electrodes. The activation energy (E_a) for ionic transport is estimated from the slope of the linear fit of the Arrhenius plot (log (σ/S cm^{-1}) vs. 1000/T plot) represented by $\sigma = \sigma_0 \exp(-E_a/kT)$, where σ_0 is the constant pre-exponential factor and E_a is the activation energy. The parameter T stands for the absolute temperature and k for the Boltzmann constant. Thermal properties are investigated by differential scanning calorimetry (DSC; Sirius 3500) and thermogravimetric analysis (TGA—SHIMADZU–DTG-60H). The ion transference number (t_{ion}) has been obtained by i–t characteristics by applying a fixed DC voltage of 10 mV across the SS|BSPE|SS cell. The linear sweep voltammetry (LSV) was performed to obtain the voltage stability window.

The impedance data is transformed into the dielectric format. Dielectric properties of the synthesized BSPEs are investigated in terms of the complex dielectric permittivity, loss tangent plot, and complex conductivity. We have also simulated the complex permittivity, loss tangent and complex conductivity plot via established theoretical expression in the complete frequency window to get a proper insight of the dielectric relaxation and its influence on the ion dynamics in the blend polymer matrix. The detail of the transformation is given in our previous report [34].

Results and discussion

X-ray diffraction (XRD) analysis

The XRD pattern of the PEO–PVP blend and with different salt contents over the range 2θ = 10°–60° is shown in Fig. 2. The fundamental peaks of the PEO are at 19° (corresponding to 120 planes) and at 23° (corresponding to 112, 032 planes) associated with the semicrystalline nature of PEO (Fig. 2a). The peaks are in good agreement with the previous reports. Several low-intense peaks of PEO are also observed at 14°, 21°, 27°, 29° [37]. The broad characteristics peaks of PVP are observed at 13° and 21°, and the absence of this in the blend polymer electrolyte confirms the blend formation [35–38]. Further addition of salt alters the peak position and intensity of the crystalline peaks (Fig. 2b–j). This indicates the

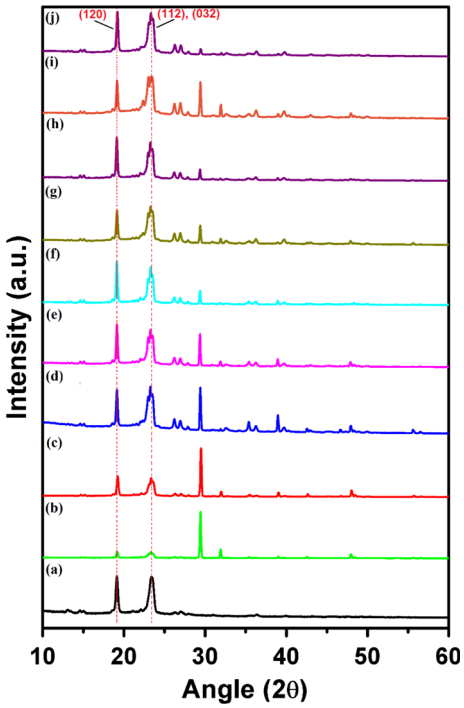

Figure 2 XRD patterns of pure PEO–PVP blend polymer with different $NaNO_3$ salt concentrations: (a) PEO–PVP, O/Na = (b) 2, (c) 4, (d) 6, (e) 8, (f) 10, (g) 12, (h) 14, (i) 16, (j) 20.

complexation between the salt and blended polymer of the prepared thin polymeric separator. The peak broadening of PEO peak infers the enhancement of the amorphous content in it. The absence of any salt peak indicates the complete salt dissociation and is in agreement with the previous literature [36]. Addition of salt shifts the peak toward the lower angle side that infers the suppression of the crystalline part and is beneficial for the fast ion migration. From the XRD spectra, structural parameters interlayer d-spacing, and interchain separation (R) are obtained for getting insights into polymer salt complex formation. The interlayer d-spacing is obtained by Braggs law $2d\sin\theta = \lambda$ and (R) using the equation $R = 5\lambda/8\sin\theta$ [27]. The increase in interchain separation and d-spacing for both the planes indicates the enhancement of the amorphous content owing to the structural modification (Table 1). It suggests (1) polymer blend formation, (2) polymer salt complexation and enhanced amorphous content, and (3) disruption of the crystalline arrangement of the polymer chain.

Table 1 Diffraction parameters for BSPE

Sample (O/Na)	120 plane			112/032 plane		
	2θ (°)	d (Å)	R (Å)	2θ (°)	d (Å)	R (Å)
PEO–PVP	19.12	4.63	5.79	23.44	3.79	4.73
2	19.17	4.62	5.77	23.29	3.81	4.76
4	19.23	4.61	5.76	23.35	3.80	4.75
6	19.13	4.63	5.79	23.25	3.82	4.77
8	19.13	4.63	5.79	23.25	3.82	4.77
10	19.13	4.63	5.79	23.25	3.82	4.77
12	19.15	4.63	5.78	23.26	3.81	4.77
14	19.12	4.63	5.79	23.24	3.82	4.77
16	19.16	4.62	5.78	23.28	3.81	4.769
20	19.19	4.62	5.77	23.32	3.81	4.760

Field emission scanning electron microscopy (FESEM) analysis

The surface morphology of the prepared polymer films has been investigated by the FESEM. Figure 3 shows the FESEM micrographs for the pure PEO (Fig. 3a), PEO–PVP blend (Fig. 3b), PEO–PVP + O/Na = 14 (Fig. 3c), and PEO–PVP + O/Na = 4 (Fig. 3d). Pure PEO shows the rough morphology that is the characteristic of the crystalline nature of the polymer, while after polymer blending, morphology get drastically changed and disappearance of the rough nature reveals the enhancement of the amorphous phase. The smooth surface is favorable for fast ionic transport, and it depicts that polymer blending has occurred as anticipated in the premise. Figure 3c shows the morphology of the optimized polymer salt matrix, and changes in the morphology confirm that complexation has been occurred in between the salt and polymer. It also suggests the

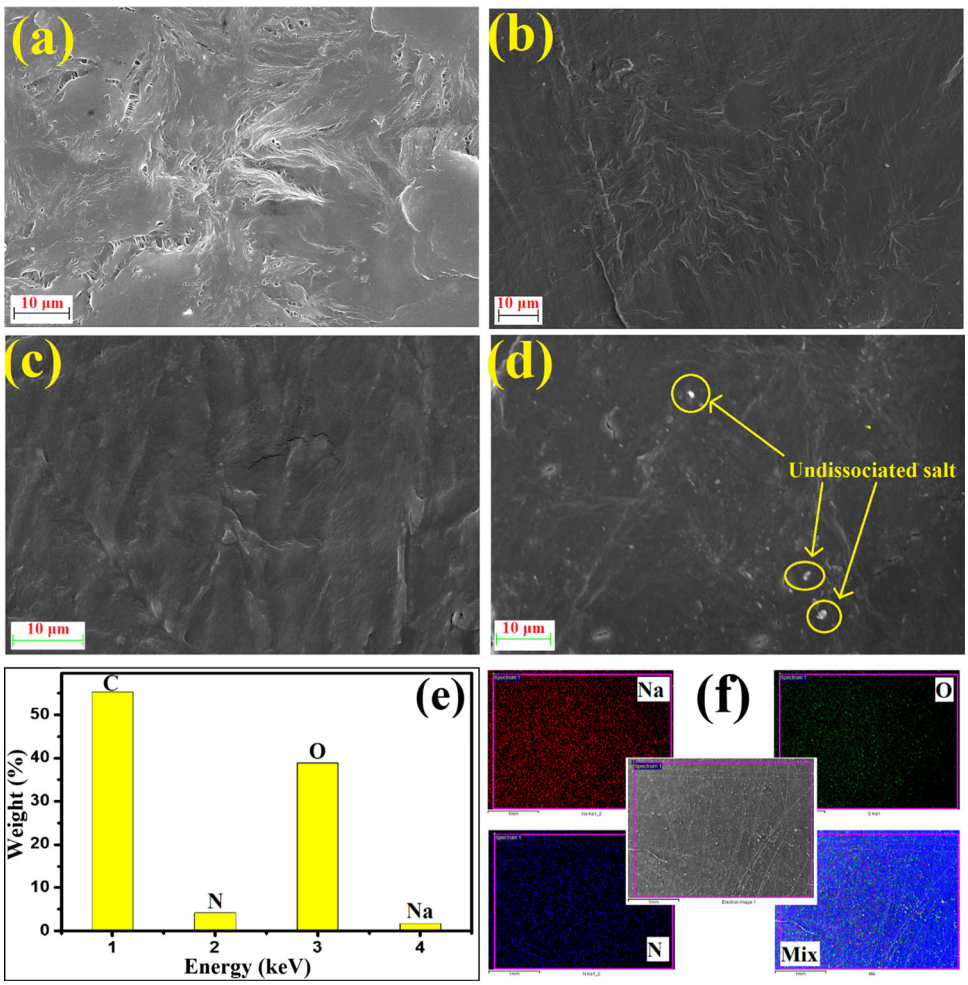

Figure 3 FESEM micrographs of **a** pure PEO, **b** blend PEO–PVP, **c** PEO–PVP + $NaNO_3$ (O/Na = 14), **d** PEO–PVP + NaNO3 (O/Na = 4), **e** EDS spectra, and **f** elemental mapping for PEO–PVP + $NaNO_3$ (O/Na = 14).

good miscibility between the polymer and salt. This is also in agreement with the XRD results. This smooth morphology and enhanced amorphous content could promote the faster ion migration [27, 39]. Figure 3d shows the morphology of the polymer salt system with higher salt content (O/Na = 4). The smooth nature of the film and overlapped nature suggests the complex formation which will support in lowering the interfacial resistance. However, the polymer film is seen to have an inhomogeneous morphology with some salt agglomeration (shown by a yellow circle) that reveals the inhomogeneous salt distribution and indicates the presence of an ion pair. Figure 3 e confirms the presence of salt in the polymer matrix (O/Na = 14) investigated in terms of EDS spectra. Further, to check the homogeneity of salt in a blend polymer matrix, elemental mapping of the Na, O, N is performed for polymer salt matrix (O/Na = 14) and confirmed the uniform salt dispersion in the complete polymer salt matrix. In brief, FESEM analysis discloses the (1) polymer blend formation, (2) polymer salt complexation occurrence, and (3) uniform dispersion of salt in an optimized system.

Fourier transform infrared spectroscopy (FTIR) analysis

Figure 4 depicts the FTIR absorption bands of PEO–PVP and PEO–PVP + $NaNO_3$ in the wavenumber region 600–3000 cm^{-1}. The variation in the characteristics groups of the polymer blend and with the addition of salt is shown by the dotted line. The band located at 842 cm^{-1} is assigned to the CH_2 rocking mode of PVP, and a minor contribution from the C–O stretching mode is associated with PEO. The band located at 952 cm^{-1} is associated with C–O stretching vibration mode of PEO. The C–C stretching mode is located at 1060 cm^{-1}. The fundamental band of the PEO is observed at 1120 cm^{-1} associated with the C–O–C stretching mode. The three important bands are: (1) at 1282 cm^{-1} associated with CH_2 asymmetric twisting, (2) at 1348 cm^{-1} CH_2 bending mode, and (3) at 1461 cm^{-1} associated with CH_2 wagging mode. Two strong absorption bands are located at 1348 cm^{-1} and 1687 cm^{-1} which correspond to C–N stretching and C=O stretching, respectively. Then two important bands associated with the C–H stretching (symmetric and asymmetric) mode of PEO are located in the wavenumber range of 2700–3000 cm^{-1} [27, 32, 40, 41]. The characteristics IR mode

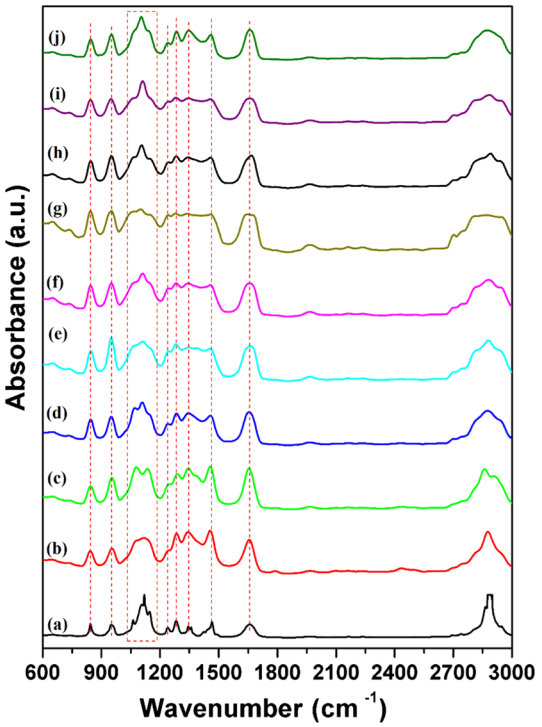

Figure 4 FTIR absorbance spectrum in the wavenumber region 600–3000 cm^{-1} for: (a) PEO–PVP, and O/Na = (b) 2, (c) 4, (d) 6, (e) 8, (f) 10, (g) 12, (h) 14, (i) 16, and (j) 20.

of anion (NO_3^-) is located at 680, and 1350 cm^{-1} in the polymer salt matrix [42]. To explore the interactions between the polymer and salt, the FTIR spectra are explained in the forthcoming section (Table 2).

Polymer–ion interaction

Figure 5 shows the magnified view of the (1) fingerprint region, 600–1500 cm^{-1}, and (2) C–H st. mode, 2700–3000 cm^{-1}. (1) *fingerprint region* Fig. 5 a shows the major absorbance bands at 842, 952, 1120, 1282, 1348, 1461 cm^{-1} associated with the CH_2 rocking/C–O stretching, C–O stretching, C–O–C stretching, CH_2 asymmetric twisting, CH_2 bending mode, and CH_2 wagging mode, respectively. It can be observed that even the addition of small amount of salt in all the blend polymer peaks shows a change in the peak intensity and shape [15, 26, 27, 29, 32]. This evidences that salt plays an effective role in altering the polymer blend system and interactions. The characteristics band of the PEO located at 1120 cm^{-1} shifts toward lower wavenumber side, and asymmetry in peak is observed. It suggests that the cation get coordinated with this and complexation between the polymer

Table 2 Band assignment and peak position of the functional group of blend solid polymer electrolyte

PEO–PVP	O/Na = 2	O/Na = 4	O/Na = 6	O/Na = 8	O/Na = 10	O/Na = 12	O/Na = 14	O/Na = 16	O/Na = 20	Band assignment
Wavenumber (cm^{-1})										
842	842	844	844	844	846	842	845	842	845	CH_2 rocking
952	954	955	951	950	951	950	951	950	950	C–O stretching vibration
1061	1067	1072	1065	1060	1064	1051	1059	1061	1059	C–C bending mode vibration
1120	1118	1136	1109	1119	1111	1110	1105	1111	1105	Symm and asymm. C–O–C st.
1146	1141	1139	1147	1151	1147	1155	1151	1152	1145	
1238	1241	1239	1239	1239	1242	1241	1244	1239	1241	CH_2 twisting/wagging
1284	1284	1272	1285	1282	1283	1280	1280	1282	1282	CH_2 asymmetric twisting
1464	1458	1457	1465	1469	1464	1464	1466	1466	1461	CH_2 wagging
1659	1657	1653	1656	1661	1659	1665	1667	1662	1658	C=O stretching
2890	2878	2862	2878	2880	2882	2885	2890	2890	2892	C–H stretching

salts is confirmed. With the further change of salt content, this peak clearly shows the splitting in three peaks (Fig. 5b–j). This strongly evidences the polymer salt complexation, and peak broadening suggests the enhancement of the amorphous content. A new peak is observed with the addition of salt near 1240 cm^{-1} and is associated with the CH_2 symmetric/asymmetric twisting mode of PEO which also shows noticeable changes with the addition of salt. The peaks located at 1348 and 1461 cm^{-1} show a reduction of the intensity and confirm that salt plays an effective role in alerting the interactions between the polymer and salt. (2) *C–H st. mode; 2700–3000 cm^{-1}* Addition of salt in the blend polymer matrix changes the peak shape located in wavenumber region of 2700–3000 cm^{-1}. The appearance of shoulder peak (indicated by arrow) evidences the polymer salt complex formation. With the change of salt content, peak broadening is observed and PEO structure is altered due to the interaction of salt with the polymer.

It may be concluded from the above discussion and analysis that the addition of salt results in a reduction of intensity and peak broadening which infers the increase of disorder in the polymer matrix. This indicates the formation of a favorable environment for the cation migration which will be further confirmed by the impedance and the transport studies.

Ion–ion interaction

To further explore the present system, ion–ion interactions are studied by exploring the anion vibration mode (NO_3^-) which is IR active, while the cation (Na^+) is IR inactive. The NO_3^- mode exhibits the D_{3h} point group and four fundamental modes are observed, i.e., ν_1 (A_1'), ν_2 (A_1''), ν_3 (E'), ν_4 (E'). The ν_1 (symmetric stretching mode at 690/1049/1355 cm^{-1}) mode is Raman active, ν_2 mode (out-of-plane symmetric deformation mode at 830 cm^{-1}) is IR active, and ν_3 (antisymmetric stretching or degenerate mode at 1350 cm^{-1}) + ν_4 (antisymmetric deformation mode at 680 cm^{-1}) are IR + Raman active [42]. So the peak located near the most intense band at 1350 cm^{-1} is deconvoluted due to the presence of dominant asymmetry using the Voigt area function (in Peak Fit software) to examine the free anion (NO_3^-) and ion pair (Na^+–NO_3^-) contribution. The baseline correction was done prior to deconvolution. The deconvolution pattern gives two types of vibration modes due to asymmetry: one at lower wavenumber side is attributed to 'free anion' vibration (NO_3^-), while the other at higher wavenumber side is attributed to the 'ion pairs' mode (Na^+–NO_3^-) (Fig. 6). A quantitative estimation of the fraction of free anion (FFA) and fraction of ion pair (FIP) was examined from the area of deconvoluted peaks assigned to specific ions using the following equation, $\mathrm{FFA}(\%) = \frac{A_{\mathrm{free}}}{A_{\mathrm{free}}+A_{\mathrm{pair}}}$ and $\mathrm{FIP}(\%) = \frac{A_{\mathrm{pair}}}{A_{\mathrm{free}}+A_{\mathrm{pair}}}$. Here, A_{free} is the area representing free ion peak and A_{pair} area of the peak representing as ion-pair peak [43, 44]. Table 3 summarizes the corresponding free

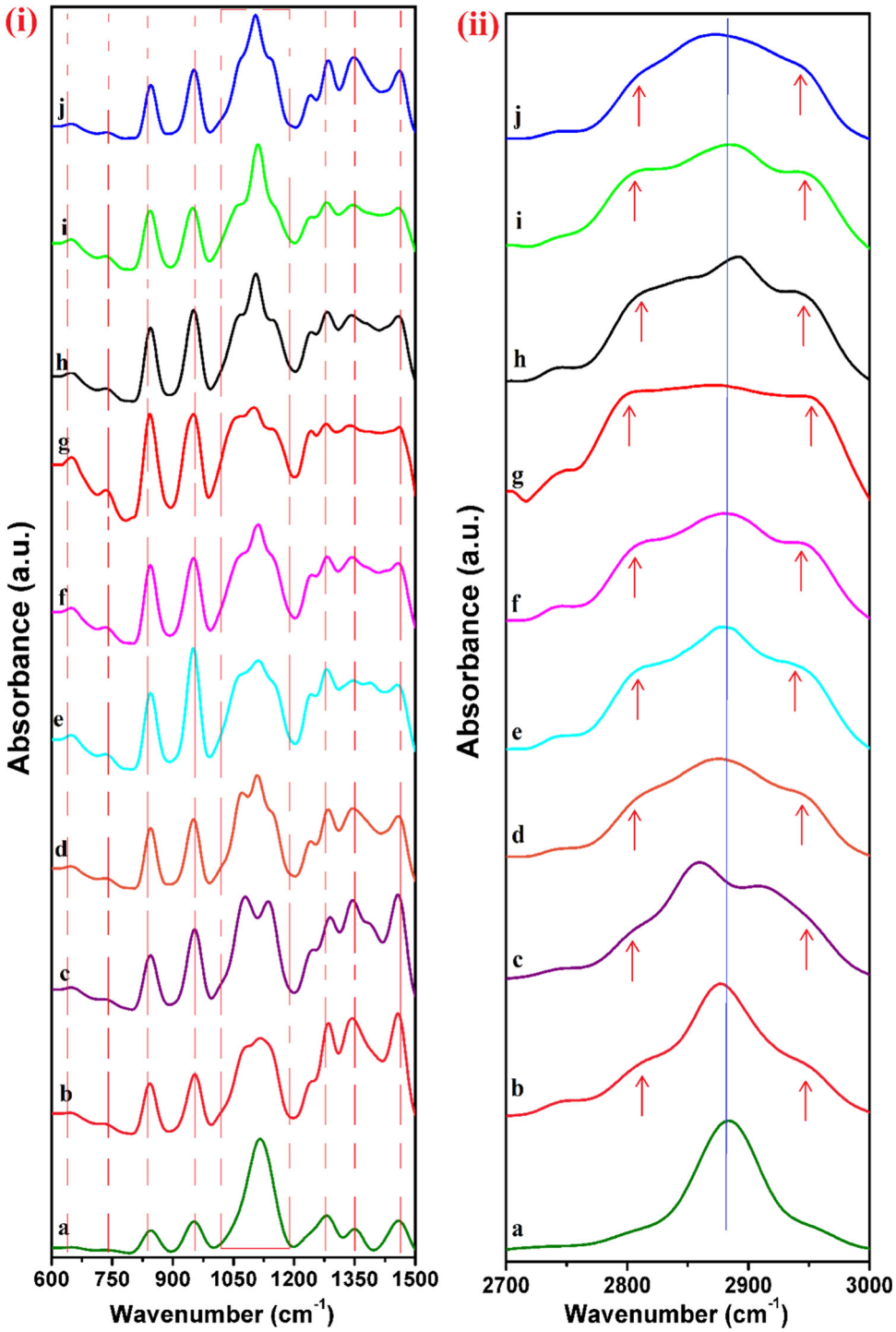

Figure 5 FTIR absorbance spectrum in the wavenumber region **i** 600–1500 cm^{-1}, and **ii** 2700–3000 cm^{-1} for O/Na (a) PEO–PVP, and O/Na = (b) 2, (c) 4, (d) 6, (e) 8, (f) 10, (g) 12, (h) 14, (i) 16, (j) 20.

ion area and ion-pair area along with peak position and value of correlation coefficient close to unity confirms the best fit.

It may be observed that the fraction of free ions varies with salt concentration and increases with salt concentration initially. Then at high content salt is not dissociated properly and ion-pair area is more as compared to the free ion area. As a high value of free ion area indicates the availability of more free ions for conduction, this directly infers the higher ionic conductivity which could be realized as discussed in the forthcoming discussion. The highest fraction of free anion is for the salt concentration which exhibits maximum conductivity (O/Na = 14). It evidences the

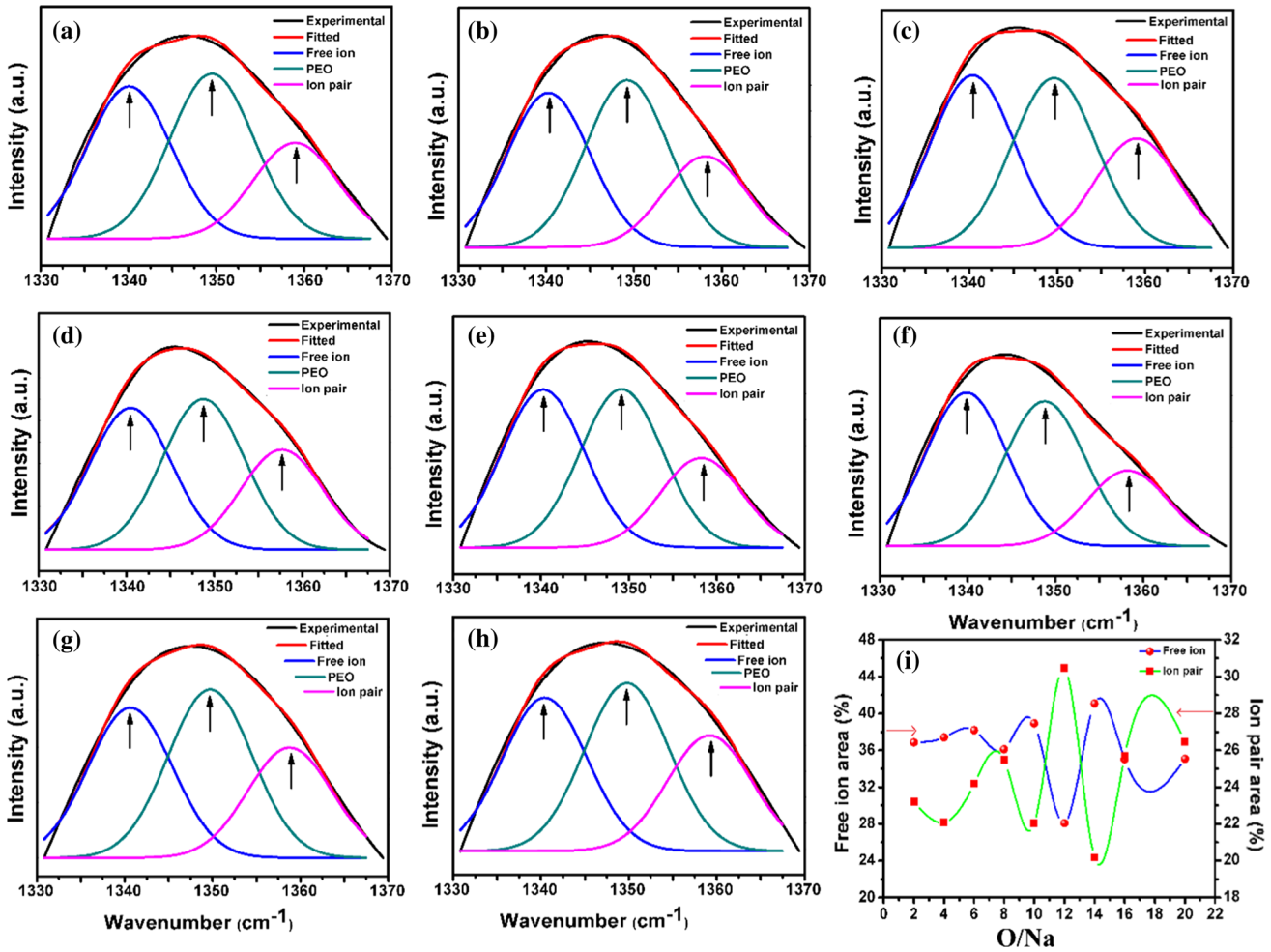

Figure 6 Deconvolution of the NO_3^- vibration mode in the wavenumber range 1330–1370 cm^{-1} for PEO–PVP + $NaNO_3$ (O/Na^+) **a** 2, **b** 4, **c** 6, **d** 8, **e** 10, **f** 14, **g** 16, **h** 20, and **f** variation of FFA and FIP against salt content.

Table 3 Peak position of deconvoluted free ion and ion-pair peak of SPE films

O/Na	Free ion		Ion-pair		Corr. coff. (r^2)
	Area (%)	Wavenumber (cm^{-1})	Area (%)	Wavenumber (cm^{-1})	
2	36.86	1340	23.20	1358	0.99
4	37.41	1340	22.07	1358	0.99
6	38.19	1340	24.19	1358	0.99
8	36.11	1340	25.48	1357	0.99
10	38.92	1340	22.02	1358	0.99
12	28.05	1338	30.46	1351	0.97
14	41.08	1340	20.16	1358	0.99
16	35.03	1340	25.71	1358	0.99
20	35.09	1340	26.46	1358	0.99

proper salt dissociation and is attributed to the creation of the most favorable environment that provides balanced interactions between polymers and salt. It may be noted that corresponding to this concentration ion pair exhibits a minimum.

Electrochemical analysis

Impedance spectroscopic analysis

The effect of salt stoichiometric ratio on the polymer blend (PEO–PVP) has been investigated on the ionic conductivity via the complex impedance spectroscopy method in the temperature range 40–100 °C. (Cell assembly SS | SPE | SS is shown in inset.)

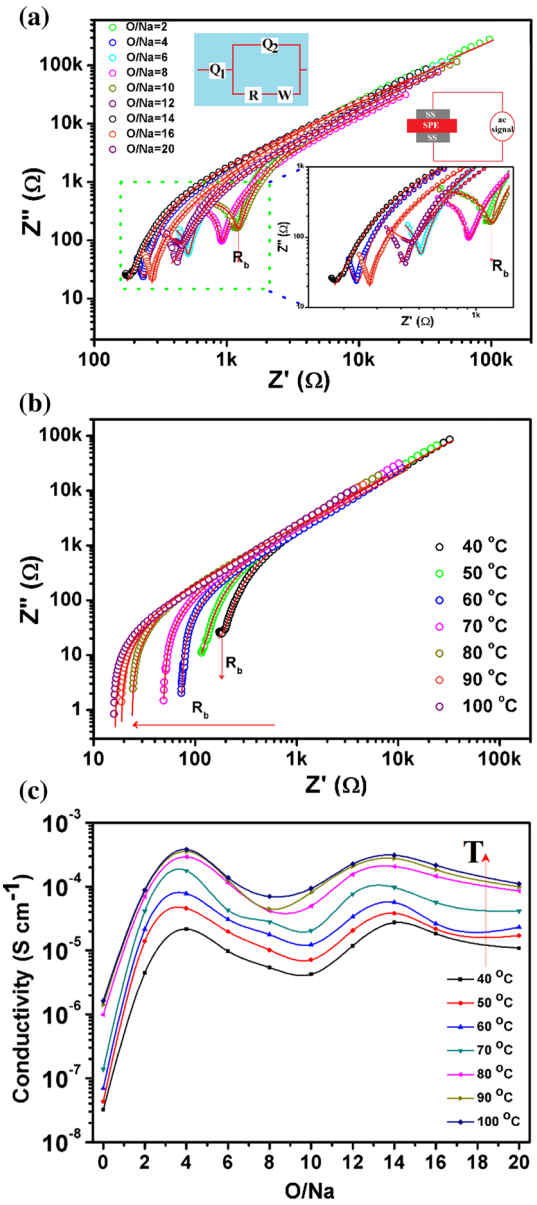

Figure 7 **a** Room-temperature log–log fitted complex impedance plot for different salt concentrations (O/Na). **b** Log–log fitted impedance plot of O/Na = 14 at a different temperatures of 40–100 °C. **c** Variation of electrical conductivity with temperature variation 40–100 °C for different salt concentrations.

Figure 7a shows the plot of imaginary part of impedance (Z'') against the real part of impedance (Z') for varied salt concentrations in log–log presentation (Nyquist plot). The plot comprises two arcs: one lying at low-frequency region corresponds to the electrode–electrolyte interface and high-frequency region arc to the bulk phenomena. The dip in the plot corresponding to the minima in the imaginary part of impedance indicates the bulk resistance (R_b) value (real part of impedance on the x-axis). It may be noted that with the addition of salt nature of arc changes. The lowering in length of high-frequency arc suggests the lowering of resistivity with salt concentration. The low-frequency arc increases in length and indicates the enhanced contribution of the electrode polarization owing to the ion accumulation on the blocking SS electrodes [45–50]. It may be noticed from the inset plot that the minima in the imaginary part of the plot is lowest for O/Na = 14 based system (inset in Fig. 7a). The solid line in the plot is the best fit performed with $Z_{SimpWin}$ software, and perfect agreement between the experimental and fitted result is obtained. (The fitted circuit is shown in inset.) It suggests that this is the optimum system and exhibits the faster ion transport and also provides approximately evidence of the highest ionic conductivity. It is discussed further in the following section.

Electrical conductivity spectrum evaluation analysis

The electrical conductivity (σ) has been obtained from the CIS spectra using the equation $\sigma = {}^{t}/_{R_b} \times A$, where '$t$' is the thickness of the SPE thin film and R_b is bulk resistance, A is the contact electrode surface area of SPE. The R_b has been obtained from the dip in the plot. It is noticed from the plot that bulk resistance decreases with varying salt contents and is lowest for the O/Na = 14 salt concentration. The electrical conductivity is summarized for different salt concentrations in Table 4. The decrease in the bulk resistance implies the highest conductivity for this concentration ($\sim 3 \times 10^{-5}$ S cm^{-1}) and is attributed to the effective interaction between the ether group and Na^+ cations in the polymer matrix. A variation of electrical conductivity is shown in Fig. 7b for the optimum concentration. It shows the disappearance of the high-frequency arc with temperature and the low-frequency arc is more dominating. It is indicated the thermal activation of charge

Table 4 Bulk conductivity, ion transference number, ionic/electronic conductivity contribution, voltage stability window and activation energy for the prepared blend solid polymer electrolyte

O/Na	Bulk conductivity (S cm^{-1})		Transport number		Conductivity (S cm^{-1})		ESW (V)
	(at 40 °C)	(at 100 °C)	t_{ion}	t_{elec}	σ_{ionic}	$\sigma_{electronic}$	
PEO–PVP	3.21×10^{-8}	1.63×10^{-6}	–	–	–	–	–
2	4.59×10^{-6}	9.15×10^{-5}	0.994	0.006	4.56×10^{-6}	2.75×10^{-8}	3.72
4	2.02×10^{-5}	3.63×10^{-4}	0.991	0.009	2.01×10^{-5}	1.82×10^{-7}	4.16
6	9.83×10^{-6}	1.39×10^{-4}	0.982	0.018	9.65×10^{-6}	1.77×10^{-7}	3.99
8	6.35×10^{-6}	8.26×10^{-5}	0.986	0.014	6.26×10^{-6}	8.89×10^{-8}	4.02
10	4.74×10^{-6}	1.05×10^{-4}	0.999	0.001	4.73×10^{-6}	4.74×10^{-9}	3.93
12	1.18×10^{-5}	2.26×10^{-4}	0.995	0.005	1.17×10^{-5}	5.92×10^{-8}	4.15
14	2.92×10^{-5}	3.32×10^{-4}	0.998	0.002	2.91×10^{-5}	5.84×10^{-8}	4.14
16	2.18×10^{-5}	2.57×10^{-4}	0.985	0.015	2.15×10^{-5}	3.27×10^{-7}	4.10
20	6.98×10^{-6}	7.07×10^{-5}	0.999	0.001	6.97×10^{-6}	6.98×10^{-9}	4.13

carriers that trigger salt dissociation, and lowering of the bulk resistance infers the enhancement of the electrical conductivity. This is attributed to the enhanced polymer chain flexibility that facilitates the faster ion migration [49]. Figure 7c shows the variation of electrical conductivity for different salt concentrations and in the broad temperature range. The electrical conductivity increases with the temperature for all salt concentrations and evidences the faster ion migration in the polymer matrix.

Thermal activation energy measurement

Figure 8 shows the plot of log σ versus $1000/T$ for different salt concentrations. It shows an Arrhenius-type behavior, and it implies that the ion dynamics is linked with the thermal activation of charge carriers. The activation energy has been obtained by fitting the plot with Arrhenius equation; $\sigma = \sigma_0 e^{-E_a/k_T}$, where σ is ionic conductivity, σ_o is a pre-exponential factor, E_a is activation energy, and 'k' is Boltzmann constant. The lowering of the activation energy suggests the highest ionic conductivity. The higher ionic conductivity is attributed to the reduction of polymer viscosity and hence increase in polymer flexibility. The thermal activation of charge carriers makes it easier for cation to jump to the next coordinating site, and simultaneous presence of enhanced free volume promotes faster ion migration. It also suggests the enhancement of the amorphous phase that is desirable requirement for the solid-state ionic conductor. The solid red line in the plot is the fitted Arrhenius plot [51–53].

The electrical conductivity is higher as compared to the other existing systems as summarized in Table 5. It confirms the suitability of the present system for the application in energy storage/conversion devices.

Ion-transport number analysis

The ion-transport number measurement for the blend solid polymer electrolyte is examined using Wagner's DC polarization technique. Figure 9 shows the plot of polarization current against the time. Initially, the higher current is total current which is the totality of the ionic and electronic currents. This is followed by the steady state with the passage of time and corresponds to the electronic current. The SS electrodes prevent the flow of ions across the external circuit, and this blockage of ions only permits the flow of electronic current. The ion-transport number has been obtained using the equation, $t_{ion} = (I_t - I_e)/I_t \times 100$, and $t_{ion} + t_e = 1$. The high value of ion-transport number (close to unity) confirms the ionic nature of the polymer films and is summarized in Table 4 [56–58].

Electrochemical stability window analysis

Figure 10 shows the linear sweep voltammetry measurement, and electrochemical stability window (ESW) is obtained. ESW enables us to obtain safe operation limit of the electrolyte in the application [59]. The voltage stability window is improved with the addition of salt and is higher than 4 V for the

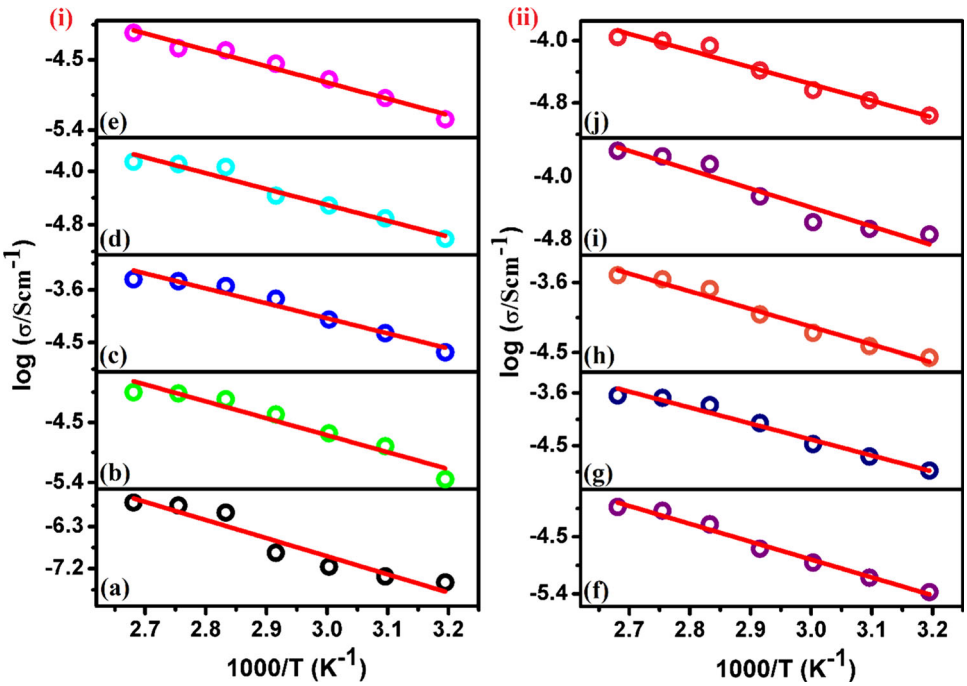

Figure 8 Arrhenius plot for (a) PEO–PVP, and O/Na = (b) 2, (c) 4, (d) 6, (e) 8, (f) 10, (g) 12, (h) 14, (i) 16, (j) 20.

Table 5 Comparison of ionic conductivity with the literature

Serial no.	Polymer	Salt	Ionic conductivity (S cm^{-1})	Temperature	References
1	PEO/PVP	NaF	1.19×10^{-7}	RT	[26]
2	PEO/PVP	$NaIO_4$	1.57×10^{-7}	RT	[31]
3	PEO/PVP	NaBr	1.90×10^{-6}	RT	[29]
4	PEO/PVP	$NaPF_6$	5.92×10^{-6}	40 °C	[27]
5	PEO/PVP	NaCl	1.66×10^{-7}	RT	[54]
6	PEO/PEMA	$NaClO_4$	6.67×10^{-7}	30 °C	[55]
7	PEO/PVP	$NaNO_3$	2.92×10^{-5}	40 °C	Our work
8	PEO/PVP	$NaNO_3$	2.90×10^{-4}	100 °C	Our work

optimized system that is in the desirable limit for the energy storage devices application [60, 61]. Table 4 summarizes the voltage stability window for BSPE.

Differential scanning calorimetry (DSC) analysis

Figure 11a–h shows the differential scanning calorimetric pattern of the blended polymer without salt and with different stoichiometric salt ratio free-standing solid films. It is important to note here that the lower value of the melting point (T_m) and crystallinity (X_c) clearly imply the enhanced polymer flexibility and favor the ion dynamics in terms of faster ion migration via coordinating sites of the polymer chain. It may be noted from Fig. 11a that the blended polymer without salt shows the melting peak located at 71.71 °C and with the addition of small amount of salt peak shifts toward lower temperature (Table 6). This evidences the polymer salt complex formation which is attributed to the interaction between the Lewis base ether group and Lewis acid cation. This also suggests the disruption of polymer chain arrangement and disorder produced in matrix enhances the ion mobility. With further addition of salt, peak shifts toward lower temperature and suggests the complexation between polymer and salt. The melting peak is lowest for the blend polymer system with the highest ionic conductivity (Fig. 11f). However, at high salt content again some shift toward high temperature is observed that may be associated with the poor polymer salt complexation [62].

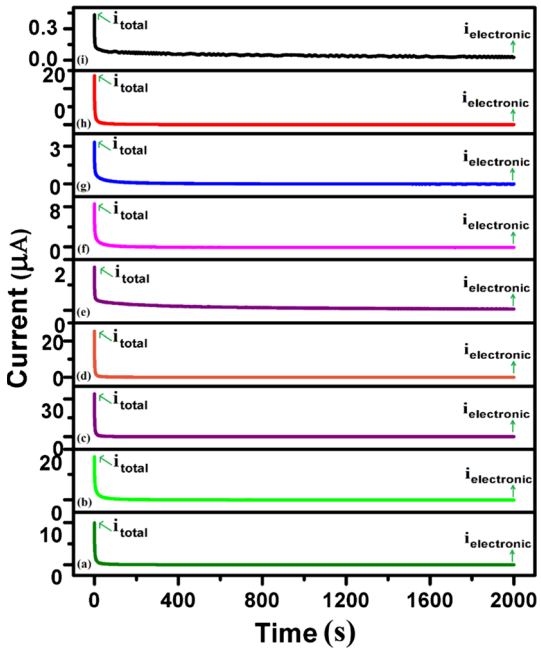

Figure 9 Ion-transport number for PEO–PVP + $NaNO_3$ in O/Na (a) 2, (b) 4, (c) 6, (d) 8, (e) 10, (f) 12, (g) 14, (h) 16, (i) 20.

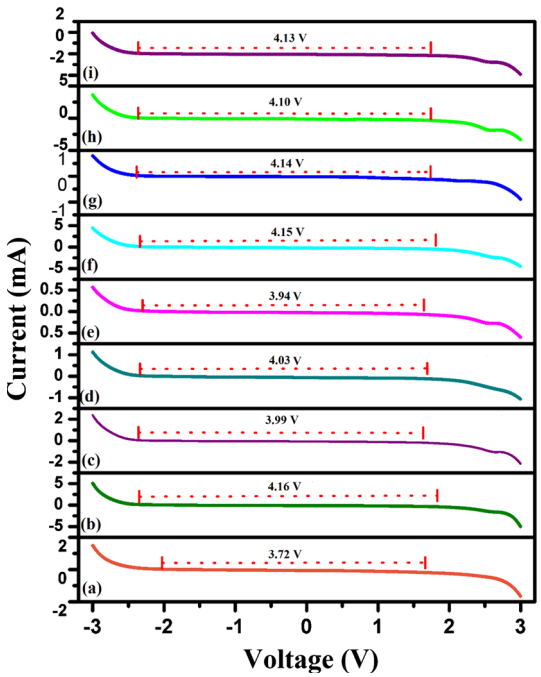

Figure 10 Linear sweep voltammetry measurement for PEO–PVP + $NaNO_3$ in O/Na (a) 2, (b) 4, (c) 6, (d) 8, (e) 10, (f) 12, (g) 14, (h) 16, (i) 20.

In order to further corroborate the DSC analysis with the above-analyzed XRD results, the crystallinity of the without and with different content of salt, freestanding solid polymeric films has been

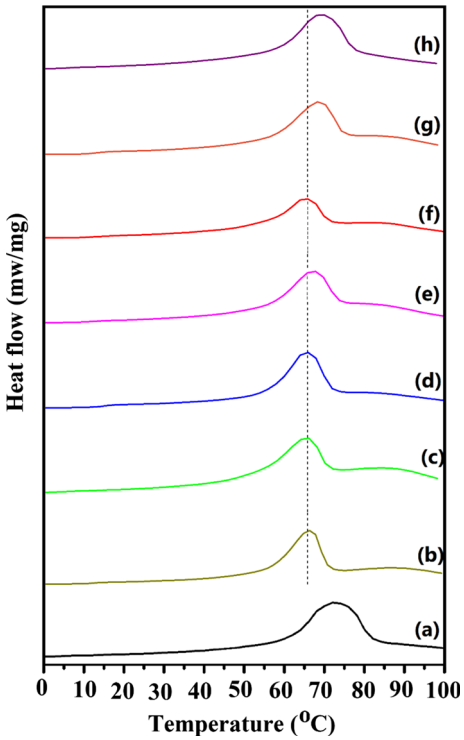

Figure 11 DSC thermograms for the solid polymer electrolytes PEO–PVP + $NaNO_3$ in (a) PEO–PVP, O/Na = (b) 2, (c) 4, (d) 6, (e) 12, (f) 14, (g) 16, (h) 20.

Table 6 Thermal properties of the blend polymer with different salt contents

O/Na	T_m (°C)	X_c (%)
PEO–PVP	71.71	56.11
2	66.23	32.51
4	65.45	21.79
6	66.78	40.06
10	66.65	30.18
12	68.12	39.66
14	65.13	20.72
16	69.17	36.79
20	69.20	54.36

analyzed and recorded systematically. It is very important and endorsement of the recorded XRD results in terms of the percentage amorphous content in the polymer after polymer salt complexation, as the evaluation of the percentage of crystallinity (%X_c) is so crucial. Therefore, the percentage of crystallinity has been calculated using equation; $X_c = \frac{\Delta H_m}{\Delta H_m^o} \times 100$, where ΔH_m is the melting enthalpy obtained from the DSC measurement and ΔH_m^o is the melting enthalpy of pure 100% crystalline PEO (188 J/g) [63].

It is noticed from Fig. 11 that the area of the peak is the lowest (Fig. 11f) for the polymer salt system

exhibiting highest ionic conductivity (Table 6). It is also clear that the crystallinity with the addition of salt decreases as compared to the polymer blend which infers the enhanced free volume. This increment of free volume size in the films certainly improves segmental motion of polymer chains that infers the faster cation migration from one coordinating site to another. The calculated results of all the samples are recorded in Table 6 confirming that the addition of salt plays an effective role in the enhancement of the amorphous content and polymer flexibility both (Fig. 11f). The simultaneous presence of both the achievement overall promotes the faster ion dynamics in the matrix. The above results are also in perfect agreement with the XRD, fraction of free ion, impedance study, and ion-transport parameters.

Thermogravimetric (TG) analysis

For safe operation of energy device, thermal stability checking is crucial before its use. The thermogravimetric (TG) curves of the blend polymer with and without salt are shown in Fig. 12. The initial weight loss is about 7.3%, 3.4% for the blend polymer (PEO–PVP, i.e., O/Na = 0) and blended polymer with salt (O/Na = 14), respectively. This is attributed to the evaporation of solvent and moisture content in BSPE films. At higher temperature, further weight loss is observed and at high temperature, (at 370 °C) weight loss is 10.33%, 8.22% for the blend polymer (without salt) and blend polymer with salt (O/Na = 14), respectively. It may be noted that the blend polymer electrolyte with salt shows the improved thermal stability inferred by low weight loss (shown by the arrow). Addition of salt slows down the process of polymer decomposition and reflects the enhanced stability range. After this temperature (i.e., 370 °C), rapid weight loss is observed that is associated with the polymer matrix decomposition followed by steady plot after 450 °C. It may be concluded that the high thermal stability of BSPE films (∼ 400 °C) is suitable for the application in sodium-ion batteries operating at high temperature (than room temperature) [64].

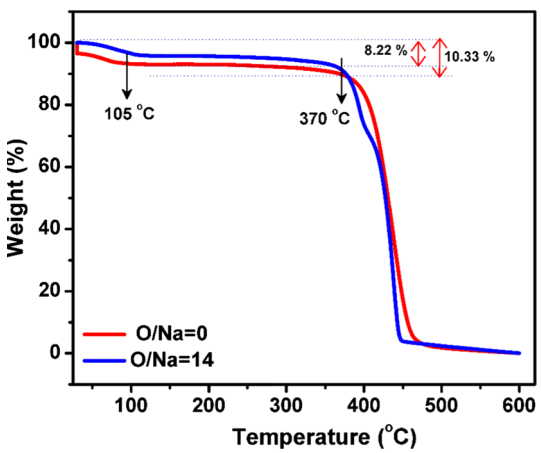

Figure 12 TGA thermograms of blend polymer without salt (PEO–PVP) and with salt for the optimized system (O/Na = 14).

Dielectric spectroscopy

Complex dielectric permittivity

The complex dielectric permittivity is expressed as $\varepsilon^* = \varepsilon' - j\varepsilon''$, where ε' is the real part and ε'' is imaginary part of the dielectric permittivity. The former one is associated with the polarizing ability or storage capacity of material and latter one corresponds to the energy loss [65]. The real part and imaginary part are expressed by the equation as $\varepsilon' = \frac{-Z''}{\omega C_o(Z'^2+Z''^2)}$ and $\varepsilon'' = \frac{Z'}{\omega C_o(Z'^2+Z''^2)}$. Here, Z' is real part of impedance, Z'' is imaginary part of impedance, $\omega = 6.28 \times f$ is angular frequency, and $C_o = \varepsilon_o A/d$ is capacitance. The real and imaginary parts are also written in extended from as Eq. 1

$$\varepsilon' = \epsilon_\infty + \frac{\Delta\varepsilon\left(1 + x^\alpha \cos\frac{\alpha\pi}{2}\right)}{1 + 2x^\alpha \cos\frac{\alpha\pi}{2} + x^{2\alpha}} \tag{1a}$$

$$\varepsilon'' = \Delta\varepsilon \frac{x^\alpha \sin\frac{\alpha\pi}{2}}{1 + 2x^\alpha \cos\frac{\alpha\pi}{2} + x^{2\alpha}} \tag{1b}$$

where ε_s is dielectric constant for $x \to 0$, ε_∞ is dielectric constant for $x \to \infty$, $x = \omega\tau$; ω is angular frequency of applied field and τ is average Debye relaxation time. Here, α is distribution exponent of material sample.

Figure 13a shows the frequency-dependent real part of the dielectric permittivity against the frequency. The plot shows the decrease in dielectric constant with an increase in the frequency for all SPE systems. On close examination, it is noticed that the dielectric constant is higher for the polymer salt system as compared to the salt-free blend polymer films. This enhancement of the dielectric constant indicates the salt dissociation into cations and anions owing to the interactions between polymer and salt. The high value of the dielectric constant in the low-frequency window is due to the dominance of the electrode polarization region when a

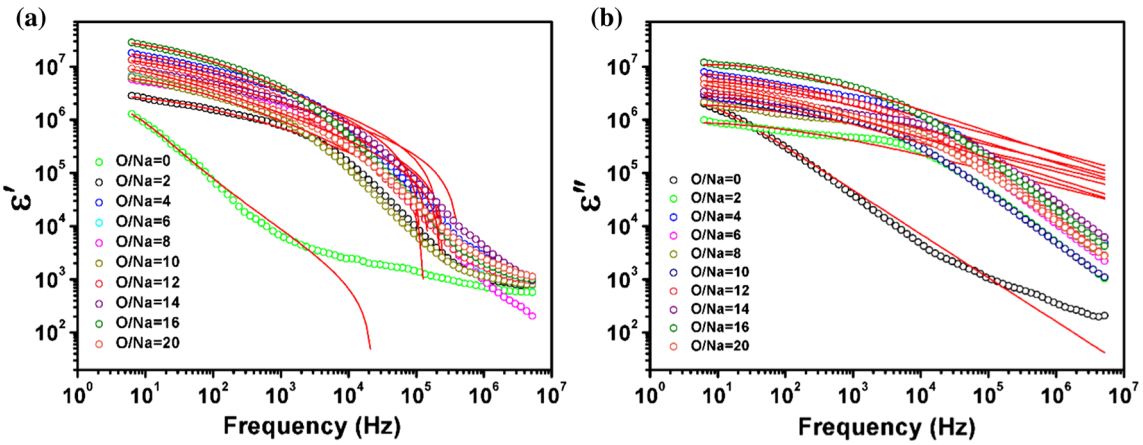

Figure 13 Frequency-dependent **a** real part and **b** imaginary part of complex permittivity for PEO–PVP + $NaNO_3$ in O/Na (= 0 (PEO–PVP), 2, 4, 6, 8, 10, 12, 14, 16, 20). The solid red line is the fitted plot.

time-dependent electric field is applied. It results in the accumulation of the ions on the electrode–electrolyte interface due to the availability of sufficient time for ion diffusion [59, 65–67]. Now, when we move from left to right in the plot (low frequency to high frequency), the decrease in dielectric constant and change in slope at an intermediate frequency is observed. The fundamental reason behind this is the dominance of the dielectric relaxation processes in the polymer matrix. This results in the decrease in a number of ion accumulation which directly reduces the dielectric constant. Actually, in the high-frequency window, the rapid switching of field direction generates a negative environment for the dipole alignment and dipoles due to lack of the sufficient time for rotation/orientation on the application of field are unable to contribute in polarization or ion accumulation. The overall effect is blockage of ion diffusion and hence decrease in dielectric constant [68–72]. The high value of dielectric constant indicates the enhancement of the ionic conductivity and follows the relation $\sigma_i = \sum_i q_i n_i \mu_i$. The effective interactions between the polymer and salt result in better salt dissociation and higher ionic conductivity.

Figure 13b shows the frequency-dependent imaginary part of the complex dielectric permittivity, and solid lines in the plot are the best fit. It also shows the same trend as real part of complex permittivity. As in the polymer electrolytes, ions are the diffusion species that responds on the application of the field. When the field direction changes, the ion dynamics is as follows; when field direction is changed, the ion gets de-accelerated, followed by a steady state. Thereafter again ion gets accelerated in the opposite direction. This results in the generation of heat inside a matrix that is known as a dielectric loss. The decrease in dielectric loss at high salt content is due to ion association owing to the strong Coulomb interaction [73, 74].

Loss tangent analysis

The loss tangent plot shows the variation of the loss tangent against the frequency and is the ratio of imaginary part of permittivity to the real part of permittivity. The plot shows an increase in the loss with frequency, followed by a maximum at any particular frequency, and then again decrease in the high frequency (Fig. 14). The low-frequency region

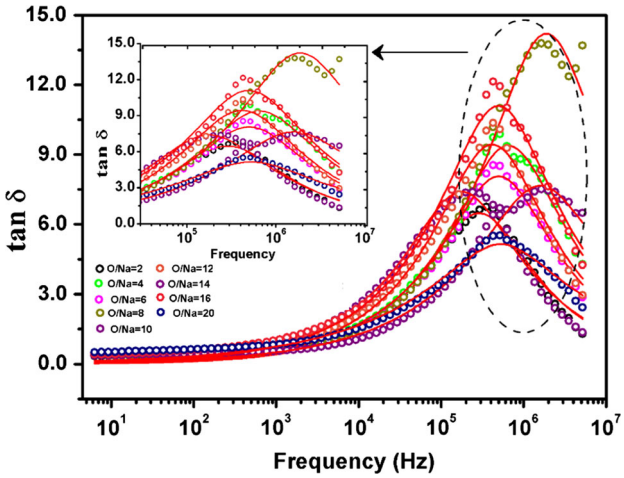

Figure 14 Tangent delta loss (tanδ) versus frequency-dependent curve for PEO/PVP + $NaNO_3$-based blend polymer electrolyte. The solid red line is the fitted plot.

(left side of the peak) is associated with the dominated Ohmic component and maxima at a particular frequency (relaxation frequency) are observed where the frequency of applied electric field matches with the frequency of molecule rotation. At this frequency, maximum power transfer occurs. This is the high-frequency region which is associated with the dominated capacitive behavior [72, 75, 76].

The effect of salt concentration is investigated on the loss tangent peak. It is noticed that the addition of salt shifts the peak toward the high-frequency side. This indicates the lowering of relaxation time owing to the faster ion migration through the coordinating sites provided by polymer backbone. The highest frequency relaxation is corresponding to the polymer salts system which exhibits the highest conductivity. The reduction of relaxation time is attributed to the enhanced polymer chain flexibility which makes easier cation migration associated with the segmental motion of the polymer chain. Further to obtain more insights, the loss tangent plot is fitted with the proposed equation in our previous report [77]. The proposed equation is obtained by modifying the Debye equation which fails to fit the plot in low-frequency window [78]. The proposed equation agrees well with experimental results in whole frequency window. The equation is expressed as, $\tan\delta = \left(\frac{(r-1)}{r+x^2}x\right)^{\alpha}$, where r is the relaxation ratio ($\varepsilon_s/\varepsilon_\infty$), ε_s is static dielectric constant ($x \to 0$), ε_∞ is dielectric constant ($x \to \infty$), $x = \omega\tau$; ω is the angular frequency of applied field and τ is Debye relaxation time (reciprocal of jump frequency in the absence of external electric field). The solid line is the best fit to the experimental results, and all shows perfect agreement with experimental results. The relaxation time obtained from the fitting is used to obtain transport parameters as summarized in the forthcoming section.

Complex conductivity analysis

The complex conductivity is expressed as, $\sigma(\omega) = \sigma' + i\sigma''$, where $\sigma'(=\omega\varepsilon_v\varepsilon'')$ is the real part of conductivity, σ'' $(=\omega\varepsilon_v\varepsilon')$ is the imaginary part of conductivity.

Sigma representation

Sigma representation plot comprises the imaginary part of complex conductivity (σ'') against the real part of complex conductivity (σ') with frequency as the variable parameter. The ideal plot shows a semicircle with two intercepts as: σ_o, σ_∞ on x-axis, respectively [79]. The diameter of the semicircle shows inverse relationship with the relaxation time and is expressed as $D = \frac{\varepsilon_v(\sigma_o-\sigma_\infty)}{2\tau}$. When imaginary part of conductivity approaches to zero corresponding to two intercepts, (1) low-frequency intercept depicts DC conductivity (σ_o) and (2) high-frequency intercept provides σ_∞ (Fig. 15). The presence of semicircle in the plot confirms the Debye nature of the investigated system. The nature of plot remains same, but the spike in the plot and diameter changes with variations of salt concentrations are clearly visible. The diameter of the semicircle is highest for the optimized system having highest ionic conductivity. The highest diameter value deduces the lowest relaxation time for this concentration, which is in good agreement with the impedance results and loss tangent analysis [27, 80–82]. It may be concluded that the polymer salt matrix with O/Na = 14 concentration is optimized concentration for the further study for device applications.

Theoretical fitting of complex conductivity analysis

Figure 16a, b shows the frequency-dependent real and imaginary parts of complex conductivity. To study the salt concentration effect in the whole frequency, the corresponding expressions of the complex conductivity are as follows [81].

$$\sigma^*_{\text{eff}} = \left(\frac{1}{\sigma_b} + \frac{1}{i\omega C_{dl}}\right)^{-1} + i\omega C_b \tag{2}$$

The real and imaginary parts of the conductivity can be written as:

$$\sigma'(\omega) = \frac{\sigma_b^2 C_{dl}\omega^\alpha \cos\left(\frac{\alpha\pi}{2}\right) + \sigma_b (C_{dl}\omega^\alpha)^2}{\sigma_b^2 + 2\sigma_b C_{dl}\omega^\alpha \cos\left(\frac{\alpha\pi}{2}\right) + (C_{dl}\omega^\alpha)^2} \tag{3a}$$

$$\sigma''(\omega) = \frac{\sigma_b^2 C_{dl}\omega^\alpha \sin\left(\frac{\alpha\pi}{2}\right)}{\sigma_b^2 + 2\sigma_b C_{dl}\omega^\alpha \cos\left(\frac{\alpha\pi}{2}\right) + (C_{dl}\omega^\alpha)^2} + \omega C_b \tag{3b}$$

The high-frequency Jonscher power law is also included in this equation as given. The real and imaginary parts of the conductivity are expressed as:

$$\sigma'(\omega) = \sigma_b\left[1 + \left(\frac{\omega}{\omega_h}\right)^n\right] \tag{4a}$$

and

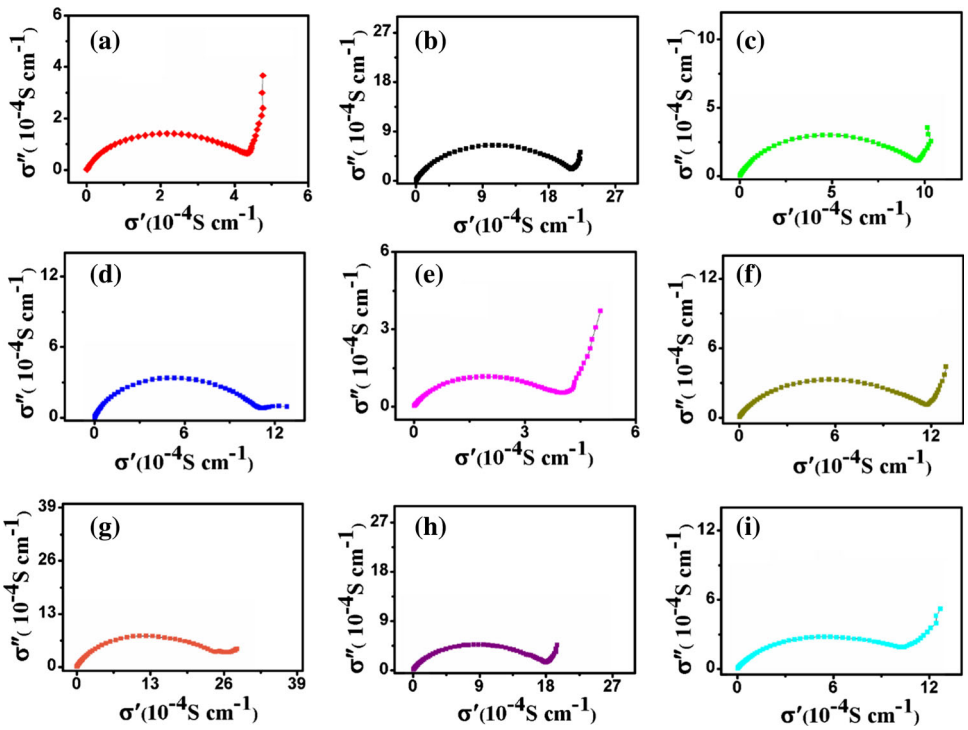

Figure 15 σ' versus σ'' plot for blend polymer PEO/PVP + $NaNO_3$-based blend polymer electrolyte in the salt concentration O/Na = (0 (PEO–PVP), 2, 4, 6, 8, 10, 12, 14, 16, 20).

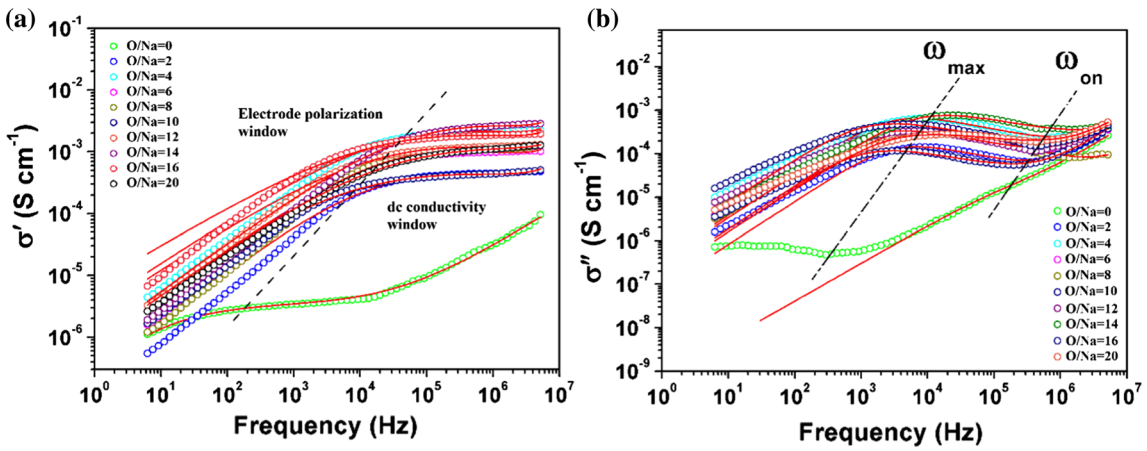

Figure 16 Frequency-dependent **a** real part of complex conductivity (σ'), and **b** imaginary part of complex conductivity (σ'' for PEO–PVP + $NaNO_3$ in O/Na (= 0 (PEO–PVP), 2, 4, 6, 8, 10, 12, 14, 16, 20). The solid red line is the fitted plot.

$$\sigma''(\omega) = A\omega^s \tag{4b}$$

Here, all parameters have their usual meaning as earlier and both 'n' and 's' have a value less than unity. For complete frequency window analysis, we replace σ_b in Eq. 3a by Eq. 4a and Eq. 3b by Eq. 4b, where C_{dl} is frequency-independent double-layer capacitance, ω is the angular frequency, s and α are exponent terms with value < 1 and C_b is the bulk capacitance of solid polymer electrolyte. The combined equations are used to fit the real and imaginary parts with the corresponding equation.

The real part of complex conductivity

The real part of conductivity against frequency comprises three regions: (1) low-frequency region associated with the electrode polarization region, (2) intermediate-frequency DC conductivity region, and (3) high-frequency dispersion region (Fig. 16a). The

low-frequency region shows the increase in the conductivity with frequency, and at intermediate frequency long-range ion migration occurs associated with cation migration from one coordinating site to another. The DC conductivity is extracted from this region. At higher frequency, the ions possess short-range path and at any particular frequency transition from long range to short range, path occurs that is termed as hopping frequency. In the high-frequency window, two competitive phenomena occur: (1) unsuccessful hopping (ion jumps back to the previous coordinating site) and (2) successful hopping (coordinating site relaxation occurs when ion achieves new site) [82–84]. The blend polymer without salt comprises all three regions, and with varying salt concentrations the high-frequency regions disappear completely, while intermediate frequency regions get shortened. This indicates the shifting of hopping frequency toward the high-frequency window associated with faster ion migration. The real part of the complex conductivity is also fitted with the equations reported somewhere [81]. The solid red line is the fitted plot and agrees well with the experimental results in the whole frequency window.

The imaginary part of complex conductivity

Figure 16b shows the frequency-dependent imaginary part of complex conductivity, and the solid red line is the fitted result which is in agreement with the experimental result in whole frequency window. The imaginary part of complex conductivity decreases when we move from right to left and a dip in the plot is obtained corresponding to onset frequency (ω_{on}). At this frequency, electrode polarization starts to build up and conductivity increases. With further decrease in frequency, peak in the plot is obtained corresponding to maximum frequency (ω_{max}). At this frequency, maximum buildup of polarization occurs. With further decrease in frequency, conductivity decreases. The same has been reported in earlier studies also [85–89]. It is important to notice here that both onset frequency (ω_{on}) and maximum frequency (ω_{max}) shift toward high-frequency side and are highest for the polymer salt matrix having highest ionic conductivity. This infers that for this concentration comparatively faster ion migrations occur and are in agreement with the loss tangent plot which shows lowest relaxation time for this system.

Transport parameters

The improved electrochemical and voltage stability properties on the addition of salt in blend polymer matrix motivated us to evaluate the transport parameters also. The transport parameters play a crucial role in the smooth facilitation of the faster ion dynamics. The fundamental transport parameters are

Table 7 Approaches to obtaining the number density (n), mobility (μ) and diffusion coefficient (D)

Units	Method		
	Bandara and Mellander (B–M) approach	Impedance spectroscopy approach	FTIR method
D ($cm^2\ s^{-1}$)	$D = \frac{d^2}{\tau_2 \delta^2}$	$D = \frac{(k_2 \varepsilon_r \varepsilon_o A d)^2}{\tau_2}$	$D = \frac{\mu k_B T}{e}$
μ ($cm^2\ V^{-1}\ s^{-1}$)	$\mu = \frac{ed^2}{kT\tau_2\delta^2}$	$\mu = \frac{e(k_2 \varepsilon_r \varepsilon_o A d)^2}{k_B T \tau_2}$	$\mu = \frac{\sigma}{ne}$
N (cm^{-3})	$n = \frac{\sigma k T \tau_2 \delta^2}{e^2 d^2}$	$n = \frac{\sigma k_B T \tau_2}{(e k_2 \varepsilon_r \varepsilon_o A d)^2}$	$n = \frac{M \times N_A}{V_{Total}} \times$ free ion area (%)
Parameters	τ_2 is a time constant corresponding to the maximum dissipative loss curve, $\delta = d/\lambda$, λ is the thickness of the electrical double layer, d is half-thickness of the polymer electrolyte	k_2 and k_1 are obtained from the trial and error on the Nyquist plot; the value of τ_2 was taken at the frequency corresponding to a minimum in the imaginary parts of the impedance, Z_i, i.e., at $Z_i \rightarrow 0$, k_B is the Boltzmann constant (1.38×10^{-23} J K^{-1}) and T is the absolute temperature	M is the number of moles of salt used in each electrolyte, N_A is Avogadro's number (6.02×10^{23} mol^{-1}), V_{Total} is the total volume of the solid polymer electrolyte, and σ is DC conductivity. e is the electric charge (1.602×10^{-19} C), k_B is the Boltzmann constant (1.38×10^{-23} J K^{-1}). T is the absolute temperature

number density of charge carriers (n), ion mobility (μ), and diffusion coefficient (D). The three methods are there to evaluate transport parameters, (1) Bandara and Mellander (B–M) approach, (2) impedance spectroscopy approach, and (3) FTIR method (Table 7). Till date, only one report is available that explored the detailed investigations and compared the transport parameters obtained by all three methods [90]. So, to strengthen the present investigation and to provide detailed analysis the transport parameters are evaluated by all methods. The mathematical equations used in evaluating the parameters are summarized in Table 7.

Figure 17 displays the variation of mobility (μ), viscosity (η) and diffusion coefficient (D) of charge carriers against the different salt contents using three different approaches (Table 8). The increase in transport parameters is associated with the following reasons: (1) reduction of crystallinity, (2) increase in segmental motion of polymer chain, (3) decrease in polymer chain viscosity, and (4) high ion conductivity. It may be noted that the transport parameters are in correlation with the XRD, fraction of free ion and impedance study. The comparison of transport parameters is also in agreement with the literature. It may be concluded that the ion dynamics is strongly influenced by the addition of the salt.

Proposed mechanism

Two-peak percolation model/mechanism

An ion-transport mechanism is proposed on the basis of the experimental evidence obtained from the FESEM, FTIR, XRD and impedance results (Fig. 18). The role of polymer and salt is explored to understand the ion dynamics.

Stage-I As the polymer blending approach was adopted to develop new polymer electrolyte. When two polymers have dissolved, the presence of hydrogen bending results in the blend formation. The blend formation is also evidenced in the FESEM and XRD analysis. Now, when salt is added in the blend polymer matrix, the salt gets dissociated into cations and anions. Now, cation has two possibilities for coordination, (1) with electron-rich group of PEO and (2) electron-rich group of PVP. But it has been confirmed in the FTIR spectra that cation is going to coordinate with the PEO as the characteristics peak (–C–O–C–) of PEO shows noticeable changes. So, in the further mechanism, only PEO chain is shown for clear representation. So, the cation gets coordinating sites from the ether group of PEO and on the application of the field migrates via these coordinating sites. However, anion due to its bulky size remains in the immobilized state and attached with polymer backbone.

Stage-II When there is lower salt content in the polymer matrix, the salt gets dissociate completely into cations and anions. So, cation migrates via the coordinating sites and contributes to conduction.

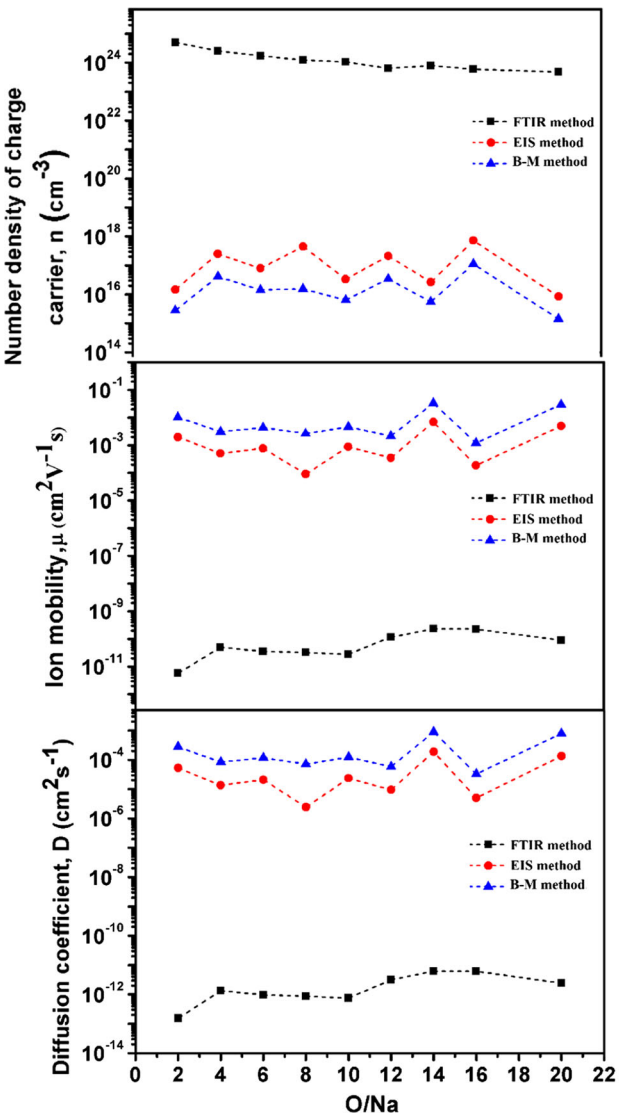

Figure 17 The diffusion coefficient, D, charge carrier mobility, μ, and charge carrier number density, n, with $NaNO_3$ salt concentration O/Na by using three methods: FTIR, EIS, and B–M methods for the PEO/PVP + $NaNO_3$ electrolyte system.

Table 8 Summary of number density (n), mobility (μ) and diffusion coefficient (D) by three approaches

O/Na	K_2 ($\times 10^7$ F^{-1})	ε_r (at 100 kHz)	τ_2 (μs)	n ($\times 10^{16}$ cm^{-3})	μ ($\times 10^{-4}$ cm^2 V^{-1} s)	D ($\times 10^{-4}$) cm^2 s^{-1}
EIS method						
2	4.52	1242.68	14.68	1.45	19.7	0.53
4	1.58	3553.95	12.12	25.09	5.05	0.12
6	2.96	1894.1	12.12	7.89	7.78	0.21
8	4.22	1332.85	17.76	45.11	0.9	0.02
10	4.51	1246.02	21.55	3.31	8.81	0.23
12	2.71	2070.08	14.68	21.17	3.48	0.09
14	0.99	5673.76	2.61	2.63	69.3	1.87
16	2.14	2625.86	14.68	72.95	1.85	0.04
20	1.8	3118.73	12.12	0.83	49.6	1.33
O/Na	$2d$ ($\times 10^{-2}$ cm)	τ_2 ($\times 10^{-4}$ s)	δ	n ($\times 10^{15}$ cm^{-3})	μ ($\times 10^{-3}$ cm^2 V^{-1} s)	D ($\times 10^{-4}$) cm^2 s^{-1}
BM method						
2	0.01	2.07	163.84	2.80	10.24	2.76
4	0.01	2.75	179.02	41.24	3.07	0.82
6	0.01	2.23	388.87	14.17	4.34	1.17
8	0.01	3.25	313.29	15.47	2.63	0.71
10	0.01	6.7	759.55	6.38	4.58	1.23
12	0.01	3.78	220.81	34.28	2.15	0.58
14	0.01	1.83	425.18	5.52	33.09	8.93
16	0.01	5.92	226.20	112.09	1.21	0.32
20	0.01	4.4	583.70	1.42	29.2	7.88
O/Na	V_{Total} (cm^3)	FIA (%)	σ ($\times 10^{-5}$) S cm^{-1}	n ($\times 10^{24}$ cm^{-3})	μ ($\times 10^{-11}$ cm^2 V^{-1} s)	D ($\times 10^{-12}$) cm^2 s^{-1}
FTIR method						
2	0.02	36.86	0.45	5.01	0.57	0.15
4	0.02	37.41	2.02	2.54	4.98	1.34
6	0.02	38.19	0.98	1.73	3.55	0.95
8	0.02	36.11	0.63	1.22	3.23	0.87
10	0.02	38.92	0.46	1.05	2.76	0.74
12	0.02	28.05	1.18	0.63	11.65	3.14
14	0.02	41.08	2.92	0.79	23.08	6.23
16	0.02	35.03	2.16	0.59	22.85	6.17
20	0.02	35.09	0.68	0.47	9.03	2.44

With further addition of salt dissociation more number of charges, carriers are available for conduction that is reflected in the maxima in the conductivity variation. This enhancement is in relation to the $\sigma = ne\mu$. This is also evidenced by the FTIR deconvolution of free ions. Now, when salt concentration is increased further (intermediate salt content), there is the tendency of the ion-pair formation and salt is not dissociated completely (shown by the green circle). This results in a decrease in the number of free ions and a decrease in conductivity is observed. With further increase in the salt content, another maximum in the conductivity is evidenced. This is associated with the additional contribution from the anions. As anion is attached with the polymer backbone and due to increased salt content, concentration gradient pushes the ion forward that also contributes to the conductivity. The increased disruption of the crystalline arrangement in the polymer matrix allows the anion movement via increased room for ion migration. Now, with the further addition of salt (high salt content), there is again a decrease in the conductivity. This decrease in the conductivity is due to the following reasons: (1)

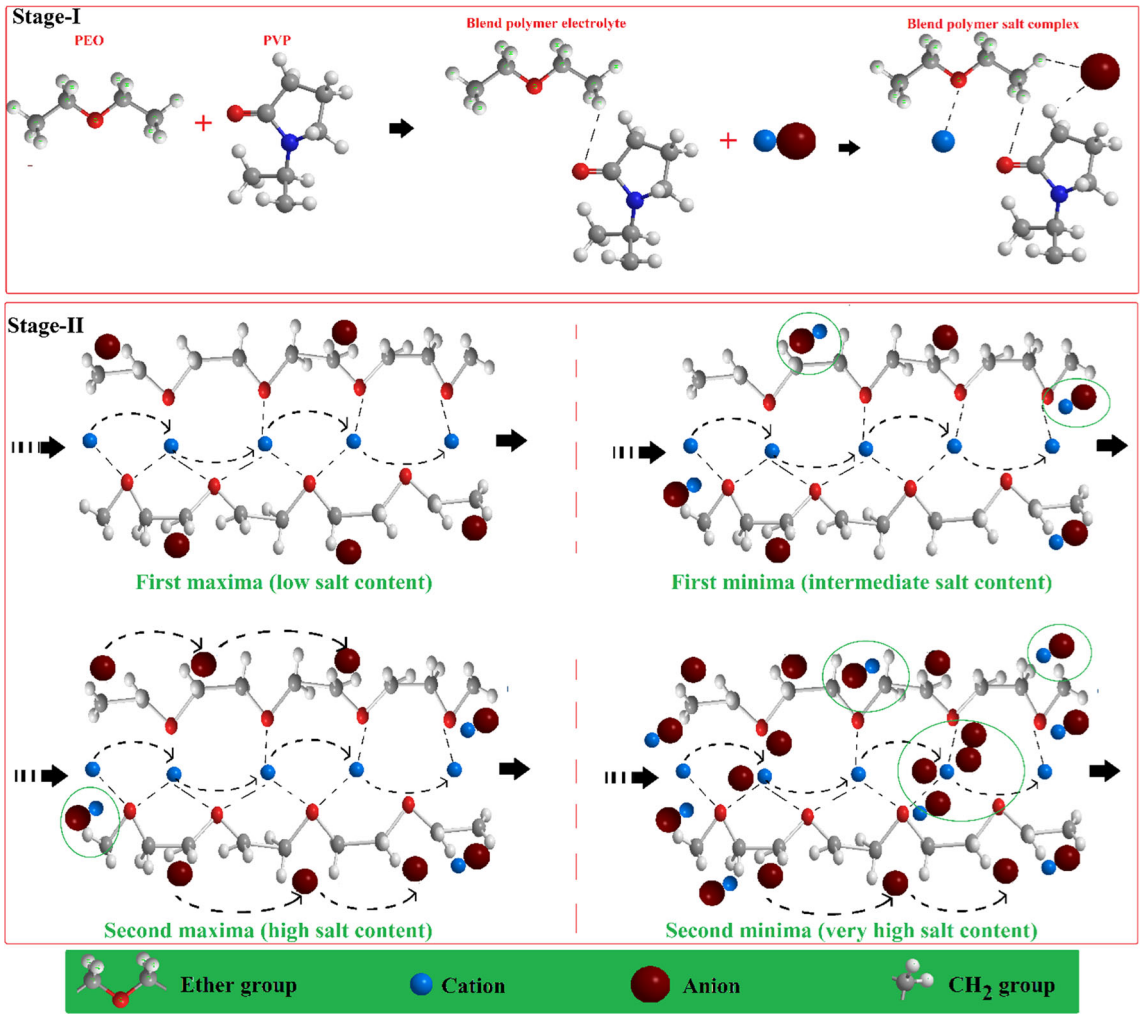

Figure 18 Proposed ion-transport mechanism in the solid polymer electrolyte.

dominance of ion-pair formation as well as ion triplets, (2) cation may trap in between the salt aggregates (shown by the green circle), (3) polymer chain reorganization tendency may enhance due to insufficient salt dissociation. The simultaneous presence of these factors results in a decrease in the conductivity and poor segmental motion. It hinders the ion migration and is also evidenced by the FESEM which shows salt agglomeration at high salt content. It may be concluded that at an optimum concentration of salt–polymer matrix is able to provide a favorable environment for cation migration with balanced interactions. The enhanced improved ionic conductivity and other desirable properties of an electrolyte strengthen its candidature for the application in the sodium-ion batteries.

Conclusion

A novel blend solid polymer electrolyte has been synthesized using the blended polymer PEO and PVP and sodium salt ($NaNO_3$) via standard solution-cast technique. The structural and microstructural changes have been analyzed through XRD and FESEM analysis. X-ray diffraction analysis indicates the reduction of crystallinity and increase in inter-chain separation evidence disruption of the covalent bonding between polymers chain which is favorable for faster ion migration. FTIR spectra confirm the complex formation and fraction of free anion increases with the addition of salt that is associated with the enhancement of a number of charge carriers. The blend polymer matrix with salt ratio O/Na = 14

exhibits the highest ionic conductivity 2.92 $\times 10^{-5}$ S cm^{-1} at room temperature and is the optimized system. This enhancement in the conductivity was attributed to the proper salt dissociation. The temperature dependence of conductivity follows the Arrhenius behavior, and conductivity increase with temperature is associated with enhanced polymer chain flexibility (2.90 $\times 10^{-4}$ S cm^{-1} at 100 °C). The ion transference number close to unity confirms the ionic nature of electrolyte, and broad voltage stability window ($\sim$ 4 V) is suitable for such applications. The decrease in melting temperature and crystallinity is evidenced from the DSC analysis which infers the increase in polymer chain flexibility which is in correlation with XRD and impedance analysis. The transport parameters have been evaluated by three methods: (1) Bandara and Mellander (B–M) approach, (2) impedance spectroscopy approach, and (3) FTIR method and are in good correlation with the literature and impedance results. The enhancement of the ion mobility and diffusion coefficient is in correlation with the impedance study. The thermal stability of the prepared film is up to 300 °C and is within a safe limit. The complex dielectric permittivity analysis evidences the enhancement of the dielectric constant with the addition of salt and indicates the enhancement of a number of free charge carriers. The loss tangent peak shifts toward higher-frequency side that implies the lowering of the relaxation time that suggests the faster polymer chain segmental motion. The sigma representation also evidences the lowering of relaxation time that is in correlation with time obtained from loss tangent analysis. The AC conductivity analysis shows an increase in DC conductivity with the addition of salt, and imaginary part of complex conductivity suggests the faster ion migration. The ion-transport mechanism has been proposed that highlights the role of polymer and salt. It may be concluded that the present BSPE has the potential to be used as an electrolyte for application in sodium-ion batteries.

Acknowledgements

One of the authors (Pritam) is thankful to CSIR, New Delhi for the award of JRF fellowship. AA is thankful to the Central University of Punjab, Bathinda, for providing fellowship.

References

[1] Yue L, Ma J, Zhang J et al (2016) All solid-state polymer electrolytes for high-performance lithium ion batteries. Energy Storage Mater 5:139–164

[2] Hasa I, Hassoun J, Passerini S (2017) Nanostructured Na-ion and Li-ion anodes for battery application: a comparative overview. Nano Res 10:3942–3969

[3] Yang Q, Zhang Z, Sun X-G et al (2018) Ionic liquids and derived materials for lithium and sodium batteries. Chem Soc Rev 47:2020–2064

[4] Saykar NG, Pilania RK, Banerjee I, Mahapatra SK (2018) Synthesis of NiO–Co_3O_4 nanosheet and its temperature-dependent supercapacitive behavior. J Phys D Appl Phys 51:475501

[5] Barbos JC, Dias JP, Lanceros-Méndez S, Costa CM (2018) Recent advances in poly(Vinylidene fluoride) and its copolymers for lithium-ion battery separators. Membranes 8:45

[6] Sim LN, Sentanin FC, Pawlicka A et al (2017) Development of polyacrylonitrile-based polymer electrolytes incorporated with lithium bis (trifluoromethane) sulfonimide for application in electrochromic device. Electrochim Acta 229:22–30

[7] Arya A, Sharma AL (2017) Polymer electrolytes for lithium ion batteries: a critical study. Ionics 23:494–540

[8] Arya A, Sharma AL (2016) Conductivity and stability properties of solid polymer electrolyte based on PEO–PAN + LiPF6 for energy storage. Appl Sci Lett 2:72–75

[9] Manuel Stephan A, Nahm KS (2006) Review on composite polymer electrolytes for lithium batteries. Polymer 47:5952–5964

[10] Manthiram A, Yu X, Wang S (2017) Lithium battery chemistries enabled by solid-state electrolytes. Nat Rev Mater 2:16103

[11] Yue L, Ma J, Zhang J et al (2016) All solid-state polymer electrolytes for high-performance lithium ion batteries. Energy Storage Mater 5:139–164

[12] Arya A, Sharma AL (2017) Insights into the use of polyethylene oxide in energy storage/conversion devices: a critical review. J Phys D Appl Phys 50:443002

[13] Janakiraman S, Padmaraj O, Ghosh S, Venimadhav A (2018) A porous poly (vinylidene fluoride-co-hexafluoropropylene) based separator-cum-gel polymer electrolyte for sodium-ion battery. J Electroanal Chem 826:142–149

[14] Zhang Z, Xu K, Rong X, Hu YS, Li H, Huang X, Chen L (2017) $Na_{3.4}Zr_{1.8}Mg_{0.2}Si_2PO_{12}$ filled poly (ethylene oxide)/$Na(CF_3SO_2)_2N$ as flexible composite polymer electrolyte for solid-state sodium batteries. J Power Sources 372:270–275

[15] Ravi M, Pavani Y, Kumar KK, Bhavani S, Sharma AK, Rao VN (2011) Studies on electrical and dielectric properties of

PVP: $KBrO_4$ complexed polymer electrolyte films. Mater Chem Phys 130:442–448

[16] Sharma AL, Shukla N, Thakur AK (2008) Studies on structure property relationship in a polymer-clay nanocomposite film based on $(PAN)_8LiClO_4$. J Polym Sci Part B Polym Phys 46:2577–2592

[17] Sharma AL, Thakur AK (2010) Improvement in voltage, thermal, mechanical stability and ion transport properties in polymer-clay nanocomposites. J Appl Polym Sci 118:2743–2753

[18] Qiao J, Fu J, Lin R, Ma J, Liu J (2010) Alkaline solid polymer electrolyte membranes based on structurally modified PVA/PVP with improved alkali stability. Polymer 5:4850–4859

[19] Rajendran S, Sivakumar M, Subadevi R (2004) Investigations on the effect of various plasticizers in PVA-PMMA solid polymer blend electrolytes. Mater Lett 58:641–649

[20] Arya A, Sharma AL, Sharma S, Sadiq M (2016) Role of low salt concentration on electrical conductivity in blend polymeric films. J Integr Sci Technol 4:17–20

[21] Arya A, Sharma S, Sharma AL, Kumar D, Sadiq M (2016) Structural and dielectric behavior of blend polymer electrolyte based on PEO–PAN + LiPF 6. Asian J Eng Appl Technol 5:4–7

[22] Bhat C, Swaroop R, Arya A, Sharma AL (2015) Effect of nano-filler on the properties of polymer nanocomposite films of PEO/PAN complexed with NaPF6. J Mater Sci Eng B 5:418–434

[23] Parameswaranpillai J, Thomas S, Grohens Y (2014) Polymer blends: state of the art, new challenges, and opportunities. In: Character Polymer Blends. Wiley

[24] Zhang X, Takegoshi K, Hikichi K (1992) High-resolution solid-state 13C nuclear magnetic resonance study on poly (vinyl alcohol)/poly (vinylpyrrolidone) blends. Polymer 33:712–717

[25] Polu AR, Kumar R, Rhee HW (2015) Magnesium ion conducting solid polymer blend electrolyte based on biodegradable polymers and application in solid-state batteries. Ionics 21:125–132

[26] Kumar KK, Ravi M, Pavani Y, Bhavani S, Sharma AK, Rao VN (2011) Investigations on the effect of complexation of NaF salt with polymer blend (PEO/PVP) electrolytes on ionic conductivity and optical energy band gaps. Phys B Condens Matter 406:1706–1712

[27] Arya A, Sharma AL (2018) Optimization of salt concentration and explanation of two peak percolation in blend solid polymer nanocomposite films. J Solid State Electrochem 22:2725–2745

[28] Chapi S, Raghu S, Devendrappa H (2016) Enhanced electrochemical, structural, optical, thermal stability and ionic conductivity of (PEO/PVP) polymer blend electrolyte for electrochemical applications. Ionics 22:803–814

[29] Kumar KK, Ravi M, Pavani Y et al (2014) Investigations on PEO/PVP/NaBr complexed polymer blend electrolytes for electrochemical cell applications. J Membr Sci 454:200–211

[30] Chandra A, Agrawal RC, Mahipal YK (2009) Ion transport property studies on PEO–PVP blended solid polymer electrolyte membranes. J Phys D Appl Phys 42:135107

[31] Koduru HK, Marino L, Scarpelli F, Petrov AG, Marinov YG, Hadjichristov GB, Iliev MT, Scaramuzza N (2017) Structural and dielectric properties of NaIO4–complexed PEO/PVP blended solid polymer electrolytes. Curr Appl Phys 17:1518–1531

[32] Kumar KN, Kang M, Sivaiah K, Ravi M, Ratnakaram YC (2016) Enhanced electrical properties of polyethylene oxide (PEO) + polyvinylpyrrolidone (PVP): Li^+ blended polymer electrolyte films with addition of Ag nanofiller. Ionics 22:815–825

[33] Arya A, Nilesh Saykar G, Sharma AL (2018) Impact of shape (nanofiller vs. nanorod) of TiO_2 nanoparticle on free standing solid polymeric separator for energy storage/conversion devices. J Appl Polym Sci 136:47361

[34] Arya A, Sharma AL (2018) Effect of salt concentration on dielectric properties of Li-ion conducting blend polymer electrolytes. J Mater Sci Mater Electron 29:17903–17920

[35] Sengwa RJ, Dhatarwal P, Choudhary S (2015) Effects of plasticizer and nanofiller on the dielectric dispersion and relaxation behaviour of a polymer blend based solid polymer electrolytes. Curr Appl Phys 15:135–143

[36] Sreekanth T, Reddy MJ, Ramalingaiah S, Rao US (1999) Ion-conducting polymer electrolyte based on poly (ethylene oxide) complexed with $NaNO_3$ salt-application as an electrochemical cell. J Power Sources 79:105–110

[37] Jinisha B, Anilkumar KM, Manoj M, Abhilash A, Pradeep VS, Jayalekshmi S (2018) Poly (ethylene oxide)(PEO)-based, sodium ion-conducting, solid polymer electrolyte films, dispersed with Al_2O_3 filler, for applications in sodium ion cells. Ionics 24:1675–1678

[38] Abdelrazek EM, Abdelghany AM, Badr SI, Morsi MA (2017) Structural, optical, morphological and thermal properties of PEO/PVP blend containing different concentrations of biosynthesized Au nanoparticles. J Mater Res Technol 7:419–431

[39] Ma Y, Li LB, Gao GX, Yang XY, You Y (2016) Effect of montmorillonite on the ionic conductivity and electrochemical properties of a composite solid polymer electrolyte based on polyvinylidenedifluoride/polyvinyl alcohol matrix for lithium ion batteries. Electrochim Acta 187:535–542

[40] Kesavan K, Mathew CM, Rajendran S, Ulaganathan M (2014) Preparation and characterization of novel solid

polymer blend electrolytes based on poly (vinyl pyrrolidone) with various concentrations of lithium perchlorate. Mater Sci Eng B 184:26–33

[41] Kesavan K, Mathew CM, Rajendran S (2014) Lithium ion conduction and ion-polymer interaction in poly (vinyl pyrrolidone) based electrolytes blended with different plasticizers. Chin Chem Lett 25:1428–1434

[42] Bertolla L, Dlouhý I, Tatarko P, Viani A, Mahajan A, Chlup Z, Boccaccini AR (2017) Pressureless spark plasma–sintered Bioglass® 45S5 with enhanced mechanical properties and stress–induced new phase formation. J Eur Ceram Soc 37:2727–2736

[43] Sharma AL, Thakur AK (2010) Polymer–ion–clay interaction based model for ion conduction in intercalation-type polymer nanocomposite. Ionics 16:339–350

[44] Sharma AL, Thakur AK (2011) Polymer matrix–clay interaction mediated mechanism of electrical transport in exfoliated and intercalated polymer nanocomposites. J Mater Sci 46:1916–1931. https://doi.org/10.1007/s10853-010-5027-x

[45] Das A, Thakur AK, Kumar K (2013) Exploring low temperature Li^+ ion conducting plastic battery electrolyte. Ionics 19:1811–1823

[46] Arya A, Sadiq M, Sharma AL (2018) Structural, electrical and ion transport properties of free standing blended solid polymeric thin films. Polym Bull. https://doi.org/10.1007/s00289-018-2645-y

[47] Qian X, Gu N, Cheng Z, Yang X, Wang E, Dong S (2001) Impedance study of (PEO)10$LiClO_4$–Al_2O_3 composite polymer electrolyte with blocking electrodes. Electrochim Acta 46:1829–1836

[48] Tang R, Jiang C, Qian W, Jian J, Zhang X, Wang H, Yang H (2015) Dielectric relaxation, resonance and scaling behaviors in $Sr_3Co_2Fe_{24}O_{41}$ hexaferrite. Sci Rep 5:13645

[49] Muchakayala R, Song S, Gao S, Wang X, Fan Y (2017) Structure and ion transport in an ethylene carbonate-modified biodegradable gel polymer electrolyte. Polym Test 58:116–125

[50] Wu XL, Xin S, Seo HH, Kim J, Guo YG, Lee JS (2011) Enhanced Li^+ conductivity in PEO–LiBOB polymer electrolytes by using succinonitrile as a plasticizer. Solid State Ionics 186:1–6

[51] Nadimicherla R, Kalla R, Muchakayala R, Guo X (2015) Effects of potassium iodide (KI) on crystallinity, thermal stability, and electrical properties of polymer blend electrolytes (PVC/PEO: KI). Solid State Ionics 278:260–267

[52] Ramesh S, Yahaya AH, Arof AK (2002) Dielectric behaviour of PVC-based polymer electrolytes. Solid State Ionics 152:291–294

[53] Zhang J, Yue L, Hu P, Liu Z, Qin B, Zhang B, Yao J (2014) Taichi-inspired rigid-flexible coupling cellulose-supported solid polymer electrolyte for high-performance lithium batteries. Sci Rep 4:6272

[54] Kumar K, Ravi M, Pavani Y, Bhavani S, Sharma AK, VVR NR (2012) Electrical conduction mechanism in NaCl complexed PEO/PVP polymer blend electrolytes. J Non Cryst Solids 358:3205–3211

[55] Naveen Kumar P, Sasikala U, Sharma AK (2013) Investigations on conductivity and discharge profiles of novel (PEO + PEMA) polymer blend electrolyte. Int J Inno Res Sci Eng Tech 2:3575–3582

[56] Fan L, Dang Z, Nan CW, Li M (2002) Thermal, electrical and mechanical properties of plasticized polymer electrolytes based on PEO/P (VDF-HFP) blends. Electrochim Acta 48:205–209

[57] Deraman SK, Mohamed NS, Subban RH (2013) Conductivity and electrochemical studies on polymer electrolytes based on poly vinyl (chloride)-ammonium triflate-ionic liquid for proton battery. Int J Electrochem Sci 8:1459–1468

[58] Laha P, Panda AB, Dahiwale S, Date K, Patil KR, Barhai PK, Das AK, Banerjee I, Mahapatra SK (2010) Effect of leakage current and dielectric constant on single and double layer oxides in MOS structure. Thin Solid Films 519:1530–1535

[59] Chen D, Cheng J, Wen Y, Cao G, Yang Y, Liu H (2012) Impedance study of electrochemical stability limits for electrolytes. Int J Electrochem Sci 7:12383–12390

[60] Sharma AL, Thakur AK (2013) Plastic separators with improved properties for portable power device applications. Ionics 19:795–809

[61] Zhu P, Yan C, Dirican M, Zhu J, Zang J, Selvan RK, Wu N (2018) $Li_{0.33}La_{0.557}TiO_3$ ceramic nanofiber-enhanced polyethylene oxide-based composite polymer electrolytes for all-solid-state lithium batteries. J Mater Chem A 6:4279–4285

[62] Kim S, Park SJ (2007) Preparation and ion-conducting behaviors of poly (ethylene oxide)-composite electrolytes containing lithium montmorillonite. Solid State Ionics 178:973–979

[63] Cimmino S, Di Pace E, Martuscelli E, Silvestre C (1990) Evaluation of the equilibrium melting temperature and structure analysis of poly (ethylene oxide)/poly (methyl methacrylate) blends. Die Makromolekulare Chemie Macromol Chem Phys 191:2447–2454

[64] Anilkumar KM, Jinisha B, Manoj M, Jayalekshmi S (2017) Poly (ethylene oxide)(PEO)–Poly (vinyl pyrrolidone)(PVP) blend polymer based solid electrolyte membranes for developing solid state magnesium ion cells. Eur Polym J 89:249–262

[65] Cole KS (1940) Dispersion and absorption in dielectrics I. Alternating current characteristics. J Chem Phys 9:341–351

[66] Tripathi AK, Thakur A Shukla, Marx DT (2018) Dielectric, transport and thermal properties of clay based polymer-nanocomposites. Polym Eng Sci 58:220–227

[67] Arya A, Sharma AL (2018) Structural, microstructural and electrochemical properties of dispersed-type polymer nanocomposite films. J Phys D Appl Phys 51:045504

[68] Chilaka N, Ghosh S (2014) Dielectric studies of poly (ethylene glycol)-polyurethane/poly (methylmethacrylate)/montmorillonite composite. Electrochim Acta 134: 232–241

[69] Sharma AL, Thakur AK (2011) AC conductivity and relaxation behavior in ion conducting polymer nanocomposite. Ionics 17:135–143

[70] Arya A, Sadiq M, Sharma AL (2018) Effect of variation of different nanofillers on structural, electrical, dielectric, and transport properties of blend polymer nanocomposites. Ionics 24:2295–2319

[71] Bose P, Roy A, Dutta B, Bhattacharya S (2017) Decoupling of segmental relaxation from ionic conductivity in [DEMM][TFSI] room temperature ionic liquid incorporated poly (vinylidenefluoride-co-hexafluoropropylene) membranes. Solid State Ionics 311:75–82

[72] Woo HJ, Majid SR, Arof AK (2012) Dielectric properties and morphology of polymer electrolyte based on poly (ε-caprolactone) and ammonium thiocyanate. Mater Chem Phys 134:755–761

[73] Dhatarwal P, Sengwa RJ, Choudhary S (2019) Effectively improved ionic conductivity of montmorillonite clay nanoplatelets incorporated nanocomposite solid polymer electrolytes for lithium ion-conducting devices. SN Appl Sci 1:112

[74] Teeters D, Neuman RG, Tate BD (1996) The concentration behavior of lithium triflate at the surface of polymer electrolyte materials. Solid State Ionics 85:239–245

[75] Singh RJ (2012) Solid state physics. Dorling Kindersley, Noida

[76] Chopra S, Sharma S, Goel TC, Mendiratta RG (2003) Structural, dielectric and pyroelectric studies of Pb1–XCaXTiO$_3$ thin films. Solid State Commun 27:299–304

[77] Arya A, Sharma AL (2018) Structural, electrical properties and dielectric relaxations in Na^+-ion-conducting solid polymer electrolyte. J Phys Condens Matter 30:165402

[78] Cao W, Gerhardt R (1990) Calculation of various relaxation times and conductivity for a single dielectric relaxation process. Solid State Ionics 42:213–221

[79] Wei YZ, Sridhar S (1993) A new graphical representation for dielectric data. J Chem Phys 99:3119–3124

[80] Kumar PS, Sakunthala A, Govindan K, Reddy MV, Prabu M (2016) Single crystalline TiO_2 nanorods as effective fillers for lithium ion conducting PVdF-HFP based composite polymer electrolytes. RSC Adv 6:91711–91719

[81] Roy A, Dutta B, Bhattacharya S (2016) Correlation of the average hopping length to the ion conductivity and ion diffusivity obtained from the space charge polarization in solid polymer electrolytes. RSC Adv 6(70):65434–65442

[82] Shukla N, Thakur AK, Shukla A, Marx DT (2014) Ion conduction mechanism in solid polymer electrolyte: an applicability of almond-west formalism. Int J Electrochem Sci 9:7644–7659

[83] Sharma AL, Thakur AK (2015) Relaxation behavior in clay-reinforced polymer nanocomposites. Ionics 21:1561–1575

[84] Choudhary S, Sengwa RJ (2015) Structural and dielectric studies of amorphous and semicrystalline polymers blend-based nanocomposite electrolytes. J Appl Polym Sci 15:132

[85] Wang Y, Sun CN, Fan F, Sangoro JR, Berman MB, Greenbaum SG, Zawodzinski TA, Sokolov AP (2013) Examination of methods to determine free-ion diffusivity and number density from analysis of electrode polarization. Phys Rev E Stat Nonlinear Soft Matter Phys 87:042308

[86] García-Bernabé A, Rivera A, Granados A, Luis SV, Compan V (2016) Ionic transport on composite polymers containing covalently attached and absorbed ionic liquid fragments. Electrochim Acta 213:887–897

[87] Klein RJ, Zhang S, Dou S, Jones BH, Colby RH, Runt J (2006) Modeling electrode polarization in dielectric spectroscopy: ion mobility and mobile ion concentration of single-ion polymer electrolytes. J Chem Phys 124:144903

[88] Arya A, Sharma AL (2018) Enhancement in dielectric properties of blend solid polymer electrolyte with variation of temp and salt concentration. Macromol Res. https://doi.org/10.1007/s13233-019

[89] Fuentes I, Andrio A, Teixidor F, Viñas C, Compañ V (2017) Enhanced conductivity of sodium versus lithium salts measured by impedance spectroscopy. Sodium cobaltacarboranes as electrolytes of choice. Phys Chem Chem Phys 19:15177–15186

[90] Arof AK, Amirudin S, Yusof SZ, Noor IM (2014) A method based on impedance spectroscopy to determine transport properties of polymer electrolytes. Phys Chem Chem Phys 16:1856–1867